Dirac point resonances due to atoms and molecules adsorbed on graphene and transport gaps and conductance quantization in graphene nanoribbons with covalently bonded adsorbates

Siarhei Ihnatsenka and George Kirczenow*

Department of Physics, Simon Fraser University, Burnaby, British Columbia, Canada V5A 1S6

(Received 21 August 2010; revised manuscript received 1 April 2011; published 28 June 2011)

We present a tight-binding theory of the Dirac point resonances due to adsorbed atoms and molecules on an infinite two-dimensional graphene sheet based on the standard tight-binding model of the graphene π-band electronic structure and the extended Hückel model of the adsorbate and nearby graphene carbon atoms. The relaxed atomic geometries of the adsorbates and graphene are calculated using density functional theory. Our model includes the effects of local rehybridization of the graphene from the sp^2 to sp^3 electronic structures that occurs when adsorbed atoms or molecules bond covalently to the graphene. Unlike in previous tight-binding models of Dirac point resonances, adsorbed species with multiple extended molecular orbitals and bonding to more than one graphene carbon atom are treated. More accurate and more general analytic expressions for the Green's function matrix elements that enter the T-matrix theory of Dirac point resonances than have been available previously are obtained. We study H, F, OH, and O adsorbates on graphene and for each we find a strong scattering resonance (two resonances for O) near the Dirac point of graphene, by far the strongest and closest to the Dirac point being the resonance for H. We extract a minimal set of tight-binding parameters that can be used to model resonant electron scattering and electron transport in graphene and graphene nanostructures with adsorbed H, F, OH, and O accurately and efficiently. We also compare our results for the properties of Dirac point resonances due to adsorbates on graphene with those obtained by others using density-functional-theory-based electronic structure calculations and discuss their relative merits. We then present calculations of electronic quantum transport in graphene nanoribbons with these adsorbed species. Our transport calculations capture the physics of the scattering resonances that are induced in the graphene ribbons near the Dirac point by the presence of the adsorbates. We find that the Dirac point resonances play a dominant role in quantum transport in ribbons with adsorbates: Even at low adsorbate concentrations the conductance of the ribbon is strongly suppressed and a transport gap develops for electron Fermi energies near the resonance. The transport gap is centered very near the Dirac point energy for H, below it for F and OH, and above it for O. We find conduction in ribbons with adsorbed H atoms to be very similar to that in ribbons with equal concentrations of carbon atom vacancies. We predict ribbons with adsorbed H, F, OH, and O, under appropriate conditions, to exhibit quantized conductance steps of equal height, similar to those that have been observed by Lin *et al.* [Phys. Rev. B **78**, 161409(R) (2008)] at moderately low temperatures, even for ribbons with conductances a few orders of magnitude smaller than $2e^2/h$.

DOI: 10.1103/PhysRevB.83.245442 PACS number(s): 72.80.Vp, 73.63.Nm, 73.20.Hb, 73.23.Ad

I. INTRODUCTION

In recent years graphene nanoribbons have been the subject of increasing experimental[1–16] and theoretical[17–49] interest. Ideal ribbons that are uniform in width and free of defects, adsorbates, and other disorder, should transmit electrons ballistically (i.e., without scattering) and consequently, as is the case for other quasi-one-dimensional (1D) ballistic nanostructures,[50] their low-temperature conductances are expected to be quantized in integer multiples of $2e^2/h$.[18,23,25,26,31–35,38–42] The ribbons that have been realized experimentally to date have been far from ballistic; consistent with theoretical work on strongly disordered ribbons[25–27,33,38,40–42] their measured conductances when a few transverse subbands are populated with electrons have been much smaller than the conductance quantum $2e^2/h$. Thus the recent experimental observation of quantized conductance steps in graphene nanoribbons by Lin *et al.*[3] at moderately low temperatures was surprising and especially so in view of the fact that the observed conductance step heights were two orders of magnitude smaller than $2e^2/h$. In a previous paper,[40] we explained this puzzling phenomenon as arising from enhanced electron backscattering near subband edge energies due to the presence of defects. This explanation is consistent with the conclusion drawn by Lin *et al.*[3] that the conductance steps that they observed were evidence of subband formation in their nanoribbon samples. In the models that we studied[40] carbon atom vacancies in the interior of the ribbon played a crucial role: They were responsible for the formation of *equally spaced* conductance steps in a range of temperatures T high enough to suppress universal conductance fluctuations but for which k_BT is smaller than the subband spacing, in agreement with the experiment;[3] here k_B is Boltzmann's constant. However, whether such vacancies were actually present in the experimental samples at the required concentrations was not determined in the experimental work of Lin *et al.*[3] and it is widely believed based on scanning tunneling microscopy[51](STM) and transverse electron microscopy[52](TEM) measurements that graphene samples can be free from carbon atom vacancies over large areas. On the other hand, it is reasonable to expect atomic and molecular species to be adsorbed on graphene ribbons prepared using presently available fabrication techniques.[41,53–58] Thus it is of interest to explore the possible role that such adsorbates may play in conductance quantization of the kind reported by Lin *et al.*[3]

A remarkable property of pristine graphene is that the electron dispersion near the Fermi energy is linear and forms Dirac-like cones in k-space centered on two points K and K' in the Brillouin zone.[59] The energy at which the density of states of graphene vanishes is known as the Dirac point. It has been suggested that impurities that strongly perturb the graphene should give rise to resonant states in the vicinity of the Dirac point and that these resonant states result in strong scattering of electrons in the graphene.[60–71] Adsorbed atoms and molecules that are covalently bonded to graphene perturb the graphene strongly and thus may be expected to give rise to such "Dirac point resonances." However, how adsorbate-induced Dirac point resonances affect electron transport in graphene *nanoribbons* is a topic that is yet to be explored theoretically or experimentally.

In this paper we generalize the previously proposed analytic theories of the impurity-induced Dirac point resonances[60–71] to the case of adsorbates on graphene whose electronic structure is described within the extended Hückel model of quantum chemistry.[72] The extended Hückel model[50] is a semiempirical tight-binding scheme that provides a simple but reasonably realistic description of the electronic structures of many molecules. It has been used successfully in explaining and predicting experimental transport properties of a variety of molecular systems,[50] including conduction in molecular wires bridging metal contacts[73–79] and molecular arrays on silicon[80–82] and the electroluminescence,[83] current-voltage characteristics,[83] and STM images[84] of molecules on complex substrates. Thus it offers a natural way to extend the standard tight-binding model of pristine graphene[59] to the case of graphene with adsorbates.

Here we develop a tight-binding model of graphene with adsorbates based on extended Hückel theory and use it to carry out quantum transport calculations for graphene nanoribbons with adsorbates. An important advantage of our approach is that it includes *multiple* atomic or molecular orbitals of the adsorbed species as well as the relevant non-π graphene orbitals explicitly in the tight-binding model used to calculate the effect of Dirac point resonances on transport whereas other tight-binding transport calculations[64,70,71] (which have been for *two dimensional (2D) graphene* with adsorbates or impurities) have been restricted to much simpler *single*-orbital models of Dirac point resonances.

As specific examples of adsorbates we consider H, F, and O atoms and OH groups, species that may have been present in the experimental samples of Lin *et al.*[3] that were made by oxygen plasma reactive ion etching using a hydrogen silsesquioxane etch mask that was later removed in a hydrofluoric acid solution.

We estimate the relaxed geometries of these adsorbates and carbon atoms to which they bond using *ab initio* density functional calculations.[85] It is energetically favorable for the graphene carbon atoms to which adsorbed species bond to move out of the graphene plane toward the adsorbate by fractions of an angstrom, and partial rehybridization of the carbon atom from sp^2 to sp^3 bonding then occurs.[41,53,68,86] Therefore in our treatment of the Dirac point resonances we include the atomic valence orbitals of the carbon atoms that are involved in the sp^3 bonding *in addition* to the atomic valence orbitals of the adsorbed species and the $2p_z$ orbitals of the graphene carbon atoms that are included[59] in the standard tight-binding model of graphene. Our theory also applies to species that bond simultaneously to more than one graphene carbon atom as is the case for an adsorbed O atom.

We develop more accurate and more general analytic expressions than have been available to date[60–71] for the matrix elements of the Green's function of pristine graphene that enter the theory of the Dirac point resonances and check their accuracy by numerical calculations. We then calculate the matrix elements of the T-matrix that describes the scattering of graphene electrons by the adsorbate as a function of energy and thus determine the energies at which the Dirac point resonances of the various adsorbates occur as well as the resonance energy profiles.

For each of the H, F, and OH adsorbed species we find a strong resonance located near the Dirac point. For the adsorbed O atom we find the T-matrix to exhibit a more complex energy profile with a pair of overlapping resonances of different widths near the Dirac point. For each of these adsorbed species we also develop a minimal set of tight-binding parameters that yield an accurate description of its Dirac point resonance(s). These parameter sets are used in our transport calculations on graphene nanoribbons that we report here and are expected also to be useful in other theoretical work such as studies of the tunneling spectra of adsorbates on graphene that may be observed in scanning tunneling spectroscopy experiments.

We show that Dirac point resonances due to adsorbates have a strong signature in the transport characteristics of graphene nanoribbons that depends strongly on the adsorbed species even at low adsorbate concentrations. We investigate the possible influence of adsorbates on the quantized conductances that have been observed experimentally[3] in graphene nanoribbons at moderately low temperatures and that we have studied theoretically previously[40] in models of graphene nanoribbons with vacancies. The results obtained here regarding adsorbate-induced Dirac point resonances in graphene also provide a physical interpretation of key features of the calculated nanoribbon conductances that we shall present. The transport calculations that we present yield the following salient results:

(i) The adsorption of each of the species that we study on a graphene ribbon results in very strong electron scattering especially at energies in the vicinity of the Dirac point scattering resonance associated with the respective adsorbate. This in turn leads to strong suppression of the ribbon conductance and a transport gap opening up in a range of electron Fermi energies near the energy of the Dirac point resonance.

(ii) The transport gaps occur for electron Fermi energies around the Dirac point for H, below the Dirac point for F and OH, and above the Dirac point for O adsorbates. The case of O differs qualitatively from those of F and OH because O binds to two carbon atoms belonging to different graphene sublattices while the F and OH, bind to a single carbon atom.

(iii) The conductance characteristics as functions of the electron Fermi energy for ribbons with adsorbed H atoms are very similar both qualitatively and quantitatively to those of ribbons with the same concentration of carbon atom vacancies.

(iv) We predict that ribbons with each of these adsorbed species should under appropriate conditions exhibit equally spaced conductance steps at moderately low temperatures even

for adsorbate concentrations for which the conductance is much smaller than $2e^2/h$, consistent with experiment.[3]

The remainder of this paper is organized as follows. In Sec. II–VII we present a theory of the *infinite 2D* graphene sheet with adsorbed atoms or molecules. Then in Sec. VIII and IX we apply the results obtained in the preceding sections to the problem of transport in graphene *nanoribbons*. We formulate our tight-binding model of the electronic structure of adsorbed atoms and molecules on graphene in Sec. II. In Sec. III we show how the tight-binding Hamiltonians can be transformed into effective graphene Hamiltonians that include the effect of the adsorbate by generalizing previous theoretical work to the case of adsorbate species with multiple extended molecular orbitals and bonding to more than one graphene carbon atom. In Sec. IV we briefly discuss the T-matrix theory used to study Dirac point resonances in graphene analytically. In Sec. V we derive an exact relation between the graphene Green's function matrix elements that enter the T-matrix theory. We use this relation to obtain accurate analytic expressions for these matrix elements and check their accuracy by exact numerical calculations. In Sec. VI we present our results for the Dirac point resonances of H, F, and O atoms and OH groups on graphene as well as a minimal tight-binding model that accurately reproduces those results and is used in the transport calculations that we present in Sec. IX. In Sec. VI we also examine quantitatively the effect of the adsorbate-induced sp^3 rehybridization of the graphene on the Dirac point resonances and find it to be important, and especially so for adsorbed H atoms. In Sec. VII we compare our results for the properties of Dirac point resonances due to adsorbates on graphene with those obtained by others using density-functional-theory-based electronic structure calculations. In Sec. VIII we discuss the model and methodology used in our calculations of transport in graphene *nanoribbons*. In Sec. IX we present the results of our transport calculations: In Sec. IX A we discuss ribbons with H adatoms including the effects of Dirac point resonances and graphene rehybridization on transport and on the electronic density of states. Ribbons with F, OH, and O adsorbates are then considered in Sec. IX B, IX C, and IX D. We comment on conductance asymmetries of ribbons relative to the Dirac point that result from the presence of adsorbates in Sec. IX E. In Sec. IX F we focus on the topic of conductance quantization in ribbons with adsorbates. We discuss renormalization of the energies of the ribbon subbands and Dirac point due to the presence of adsorbates in Sec. IX G and the dependence of the transport gaps on the adsorbate concentration in Sec. IX H. In Sec. X we summarize our main findings and comment briefly on potential relevant experiments.

II. THE TIGHT-BINDING HAMILTONIAN

Our starting point is the simplest tight-binding model of pristine graphene[87] embodied in the Hamiltonian

$$H_0 = -\sum_{\langle i,j\rangle} t(a_i^\dagger a_j + \text{h.c.}). \tag{1}$$

Here $-t$ is the Hamiltonian matrix element between nearest-neighbor $2p_z$ carbon orbitals of the graphene lattice and $a_i^\dagger$ is the creation operator for an electron in $2p_z$ carbon orbital i. This Hamiltonian with $t = 2.7$ eV is known to describe the π-band dispersion of graphene well at energies around the Dirac point,[59,88] i.e., in the energy range of interest in this paper. We extend this tight-binding model to include the adsorbate and its coupling to the graphene carbon atoms in the following way.

We performed *ab initio* geometry relaxations based on density functional theory for the adsorbed species on the honeycomb graphene lattice using the Gaussian 09 software package.[85] The relaxed geometries calculated in this way are expected to be accurate since density functional theory has been well optimized for carrying out accurate ground-state total energy calculations on which these relaxations are based.[50] The structures studied were graphene disks of several tens of carbon atoms passivated at the edges with hydrogen, the adsorbed species being bonded to the graphene near the center of the disk. The atoms of the adsorbed species and the carbon atoms with which they bond were allowed to relax freely, the other carbon atoms being held fixed in the standard hexagonal graphene geometry with the C−C distance of 1.42 Å. The relaxed structures obtained in this way are shown in Fig. 1.[89] The tight-binding model Hamiltonian, Eq. (1), was extended to include the atomic valence orbitals of the adsorbate and their coupling to the valence orbitals of the graphene carbon atoms by calculating the relevant matrix elements within the extended Hückel model.[50]

Extended Hückel theory is formulated in terms of small basis sets of Slater-type atomic orbitals $\{|\phi_i\rangle\}$, their overlaps $S_{ij} = \langle\phi_i|\phi_j\rangle$, and a Hamiltonian matrix $\mathcal{H}_{ij} = \langle\phi_i|\mathcal{H}|\phi_j\rangle$. The diagonal Hamiltonian elements $\mathcal{H}_{ii} = \mathcal{E}_i$ are chosen to be the experimentally determined atomic orbital ionization energies $\mathcal{E}_i$. In this paper the nondiagonal elements are approximated as in Ref. 72 by $\mathcal{H}_{ij} = (1.75 + \Delta_{ij}^2 - 0.75\Delta_{ij}^4)S_{ij}(\mathcal{E}_i + \mathcal{E}_j)/2$, where $\Delta_{ij} = (\mathcal{E}_i - \mathcal{E}_j)/(\mathcal{E}_i + \mathcal{E}_j)$, a form chosen[72] for consistency with experimental molecular electronic structure data. In the standard tight-binding Hamiltonian, Eq. (1), of pristine graphene, the energy scale is chosen so that the carbon $2p_z$ orbital energy is zero whereas in extended Hückel theory[72] the carbon $2p_z$ orbital energy is the ionization energy $\mathcal{E}_{C_{p_z}} = -11.4$ eV. Accordingly, for consistency, in our extended Hückel Hamiltonian matrix we make the replacement $\mathcal{H}_{ii} \to \mathcal{H}_{ii} - \mathcal{E}_{C_{p_z}}$. Because the extended Hückel basis states

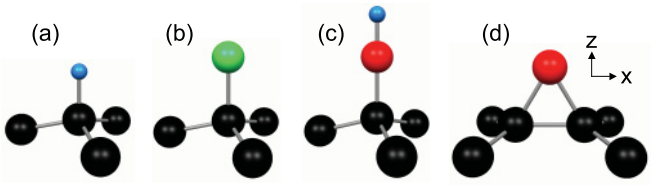

FIG. 1. (Color online) Relaxed geometries of adsorbates on graphene. C, H, F, and O atoms are black, blue, green, and red respectively.[89] (a) Adsorbed hydrogen atom. H and C atoms to which H binds are 1.47 and 0.35 Å above graphene plane. (b) Adsorbed fluorine. F and C atoms to which F binds are 1.83 and 0.36 Å above graphene plane. (c) Adsorbed hydroxyl group. H, O, and C atoms to which O binds are 2.78, 1.83, and 0.41 Å above graphene plane. (d) Adsorbed oxygen. O and C atoms to which O binds are 1.51 and 0.27 Å above graphene plane. The C atoms to which the O binds are separated by 1.47 Å. The x axis is parallel to the line joining the C atoms to which the O binds.

on different atoms are not in general mutually orthogonal the nondiagonal extended Hückel Hamiltonian matrix elements are then also adjusted according to

$$\mathcal{H}_{ij} \to \mathcal{H}_{ij} - S_{ij}\mathcal{E}_{C_{p_z}}, \tag{2}$$

as is discussed in Ref. 90.

Let $\mathcal{H}^{\mathrm{R}}_{ij}$ and S^{R}_{ij} be the extended Hückel Hamiltonian and overlap matrices defined in this way but restricted to the Hilbert subspace R spanned by the valence orbitals of the adsorbate and valence orbitals of the graphene *other than* the $2p_z$ graphene orbitals that in the present model are already described by H_0. In the numerical results presented in this paper in addition to the adsorbate valence orbitals we include in R the $2s$, $2p_x$, and $2p_y$ orbitals (see Fig. 1) of the carbon atom(s) to which the adsorbed atom or molecule bonds and of its three nearest carbon atom neighbors. We calculate $\mathcal{H}^{\mathrm{R}}_{ij}$ and S^{R}_{ij} for the relaxed geometries shown in Fig. 1. We then solve the extended Hückel Schrödinger equation

$$\mathcal{H}^{\mathrm{R}}\psi_\alpha = \epsilon_\alpha S^{\mathrm{R}}\psi_\alpha \tag{3}$$

(for a single adsorbed H, F or O atom or OH group) numerically for its eigenstates ψ_α and energy eigenvalues ϵ_α. The eigenstates ψ_α obtained in this way are mutually orthogonal. They should be regarded as *extended molecular orbitals* (EMOs) of the adsorbate. They are linear combinations of the atomic valence orbitals of the adsorbate and *some* of the atomic valence orbitals of the graphene [as is detailed above in Eq. (3)] but do *not* include any graphene $2p_z$ atomic orbitals. The EMOs will play a central role in the theory that follows.

The EMOs ψ_α together with the $2p_z$ orbitals of the graphene carbon atoms form the basis set for our tight-binding Hamiltonian H of the graphene-adsorbate system that we write in the form

$$H = H_0 + \sum_\alpha \epsilon_\alpha d^\dagger_\alpha d_\alpha + \sum_{\alpha,j} \gamma_{\alpha j}(d^\dagger_\alpha a_j + h.c.). \tag{4}$$

Here a_j is the destruction operator for an electron in the $2p_z$ orbital ϕ_j of carbon atom j. $d^\dagger_\alpha$ is the creation operator for an electron in EMO ψ_α that is an eigenstate of Eq. (3) and ϵ_α is the corresponding energy eigenvalue. $\gamma_{\alpha j} = \langle\psi_\alpha|\mathcal{H}|\phi_j\rangle$ is the matrix element of the extended Hückel Hamiltonian between the $2p_z$ orbital ϕ_j of carbon atom j and EMO ψ_α. For simplicity, in this paper we include in the sum over j in the last summation on the right-hand side of Eq. (4) only the $2p_z$ orbital of the carbon atom that is closest to the adsorbed moiety (or in the case of the adsorbed O the closest two carbon atoms), and we also neglect any changes in t in Eq. (1) that occur due to the change in the graphene geometry induced by the adsorbate. The latter effect is, however, taken into account in the numerical nanoribbon transport calculations that we report in Sec. IX.

We note that, with the above definitions, the couplings between all of the valence orbitals ($2s$,$2p_x$,$2p_y$, and $2p_z$) of the carbon atom to which the adsorbate bonds and all of the $2s$,$2p_x$,$2p_y$, and $2p_z$ valence orbitals of that carbon atom's nearest carbon atom neighbors are included in the present model that is summarized by Eq. (4). In this way we include in our calculation all of the carbon atom valence orbitals that participate in the adsorbate-induced sp^3 bonding.

Because the basis set used in extended Hückel theory is nonorthogonal, the overlap $\sigma_{\alpha j} = \langle\psi_\alpha|\phi_j\rangle$ between the $2p_z$ orbital ϕ_j of carbon atom j and EMO ψ_α may be nonzero. This overlap is neglected in Eq. (4). It has been shown[91,92] that transport problems formulated in a nonorthogonal basis can be solved by transforming to an alternate Hilbert space in which the basis is orthogonal but the effective Hamiltonian matrix elements become energy dependent. This transformation is the foundation of the standard methods used today to treat basis set nonorthogonality throughout the molecular electronics transport literature. For the present system, the transformation is accomplished by replacing $\gamma_{\alpha j}$ in Eq. (4) by $\gamma_{\alpha j} - \epsilon\sigma_{\alpha j}$. Here ϵ is the electron energy at which the Landauer electron transmission probability through the system is calculated. This correction is included in the numerical results that we present in this paper for the adsorbate-induced Dirac point resonances, although in the interests of clarity it will not appear explicitly in the formulas that we present in the remainder of this article.

III. EFFECTIVE HAMILTONIANS

In the simplest possible model of an adsorbate represented by just one atomic orbital α that couples only to the $2p_z$ orbital of only one carbon atom j of the graphene, the tight-binding Hamiltonian of the graphene and adsorbate is $H_1 = H_0 + \epsilon_\alpha d^\dagger_\alpha d_\alpha + \gamma_{\alpha j}(d^\dagger_\alpha a_j + \mathrm{h.c.})$ where the notation is as in Eq. (4). The eigenstate $|\Psi\rangle$ of H_1 with energy eigenvalue ϵ can then be written as $|\Psi\rangle = |\Psi_g\rangle + |\Psi_a\rangle$, where $|\Psi_g\rangle$ and $|\Psi_a\rangle$ are the projections of $|\Psi\rangle$ onto the space spanned by the $2p_z$ orbitals of graphene and onto the orbital of adsorbed atom, respectively. With these definitions, it has been shown[63] that $|\Psi_g\rangle$ is an exact eigenstate of an effective Hamiltonian $H_{\mathrm{eff}} = H_0 + V_j a^\dagger_j a_j$ with the same energy eigenvalue ϵ as $|\Psi\rangle$. Here $V_j = \gamma^2_{\alpha j}/(\epsilon - \epsilon_\alpha)$. Thus, for the purpose of calculating the transport coefficients of graphene with such an adsorbed atom within Landauer theory, it is sufficient to replace the Hamiltonian H_1 with H_{eff}, i.e, the Hamiltonian of graphene without the adsorbed atom but with an energy-dependent potential $\gamma^2_{\alpha j}/(\epsilon - \epsilon_\alpha)$ on carbon atom j of the graphene sheet.

We note that a general theory of systems with one or more discrete states coupled to a continuum of states was presented by Fano in 1961.[93] Graphene with an adsorbed atom or molecule is such a system. Fano's analysis of such systems[93] starts in the same way as the analysis in Ref. 64 that we have outlined above by projecting the eigenstates of the system onto the continuum and discrete state manifolds. However, unlike in Ref. 64, Fano did not reformulate the problem in terms of an effective Hamiltonian H_{eff} that acts on the continuum subspace only.[93] Subsequently, effective Hamiltonians have been employed to study bound states coupled to continua but those effective Hamiltonians have been non-Hermitian operators obtained by *eliminating the continuum subspace* from the theory,[94] unlike the Hermitian effective Hamiltonians obtained in Ref. 64 (and in the theory presented below) by *eliminating the discrete state subspace*.

In the present paper we need to include more than one extended molecular orbital ψ_α per adsorbed moiety in the tight-binding Hamiltonian given by Eq. (4) for the adsorbed

H, F, or O atom or OH group. This is the case even for H (which has only one valence orbital in extended Hückel theory) because we include several graphene atomic orbitals in the subspace R in which we calculate the EMOs ψ_α for the H adsorbate, as is discussed in Sec. II.

We find that the argument presented in Ref. 63 that leads to the effective Hamiltonian $H_{\rm eff}$ discussed above can be generalized in a direct way to adsorbates for which more than one effective molecular orbital and/or bonding of the adsorbed moiety to more than one carbon atom (as in the case of adsorbed O) must be considered.

For adsorbates with more than one extended molecular orbital that bond strongly to a single carbon atom, we find that the effective Hamiltonian still has the form $H_{\rm eff} = H_0 + V_j a_j^\dagger a_j$ but the effective potential V_j becomes $V_j = \sum_\alpha |\gamma_{\alpha j}|^2/(\epsilon - \epsilon_\alpha)$, where the sum is over the extended molecular orbitals α of the adsorbed moiety that bonds to carbon atom j of the graphene.

For a single adsorbed O atom that bonds to two neighboring graphene carbon atoms 1 and 2, the effective Hamiltonian is $H_{\rm eff} = H_0 + V_{11}a_1^\dagger a_1 + V_{22}a_2^\dagger a_2 + V_{12}a_1^\dagger a_2 + V_{21}a_2^\dagger a_1$ where $V_{nm} = \sum_\alpha \gamma_{\alpha n}\gamma_{\alpha m}^*/(\epsilon - \epsilon_\alpha)$ and the summation is over the extended molecular orbitals α of the O adsorbate. For the adsorbed O atom we consider 22 EMOs in this paper. They are linear combinations of the O $2s$, $2p_x$, $2p_y$, and $2p_z$ valence orbitals and the $2s$, $2p_x$, and $2p_y$ valence orbitals of each of the six carbon atoms shown in Fig. 1(d). The effect of the adsorbed O atom on the Hamiltonian eigenstates projected onto the graphene π-band subspace is equivalent to the combined effect of energy-dependent potentials applied to the $2p_z$ valence orbitals of the two carbon atoms to which the O atom bonds and an energy-dependent change in the Hamiltonian matrix elements between those $2p_z$ carbon orbitals.

The preceding results for the effective Hamiltonians $H_{\rm eff}$ apply equally to adsorbates on graphene nanoribbons or on 2D graphene. We now use them to develop a better understanding of how H, F, OH, and O adsorbates resonantly scatter electrons by extending the general T-matrix approach considered previously in Refs. 60,62–64,66,67,69, and 71. We consider here for simplicity the case of an isolated single H, F, OH, or O atom or molecule on infinite 2D graphene. In Sec. IX we will relate our findings to the results of our numerical transport calculations for graphene nanoribbons.

IV. T-MATRIX FORMALISM

The T-matrices that we consider are defined in the standard way by

$$G = G^0 + G^0 T G^0, \tag{5}$$

where $G = (\epsilon + i\eta - H_{\rm eff})^{-1}$ is the full Green's function based on the effective Hamiltonians $H_{\rm eff}$ discussed above for a single adsorbed atom or molecule, $G^0 = (\epsilon + i\eta - H_0)^{-1}$ is the unperturbed Green's function for π-band electrons in clean graphene, and T characterizes the scattering strength due to the adsorbate. T can be written in the standard form

$$T = \mathcal{V} + \mathcal{V}G^0\mathcal{V} + \mathcal{V}G^0\mathcal{V}G^0\mathcal{V} + \cdots, \tag{6}$$

where $\mathcal{V} = a_j^\dagger a_j \sum_\alpha |\gamma_{\alpha j}|^2/(\epsilon - \epsilon_\alpha)$ for a H, F, or OH atom or molecule with EMOs α bound to carbon atom j. For an O atom with EMOs α bound to two neighboring C atoms 1 and 2, $\mathcal{V} = V_{11}a_1^\dagger a_1 + V_{22}a_2^\dagger a_2 + V_{12}a_1^\dagger a_2 + V_{21}a_2^\dagger a_1$, where $V_{nm} = \sum_\alpha \gamma_{\alpha n}\gamma_{\alpha m}^*/(\epsilon - \epsilon_\alpha)$.

Taking matrix elements of Eq. (6) between the graphene $2p_z$ orbitals of the carbon atom(s) to which the adsorbed atom or molecule binds and summing the resulting series yields

$$\tilde{T} = (1 - \tilde{\mathcal{V}}\tilde{G}^0)^{-1}\tilde{\mathcal{V}}, \tag{7}$$

where, for the O atom adsorbate $\tilde{T}$, $\tilde{\mathcal{V}}$, $\tilde{G}^0$, and 1 are the 2×2 matrices $\langle m|T|n\rangle$, $\langle m|\mathcal{V}|n\rangle$, $\langle m|G^0|n\rangle$, and δ_{mn} with $|m\rangle$ and $|n\rangle$ being the $2p_z$ orbitals of the carbon atoms m and n to which the O atom bonds. Here $m = 1,2$ and $n = 1,2$. For H, F, and OH that bond to one C atom (labeled 1) $\tilde{T}$, $\tilde{\mathcal{V}}$, $\tilde{G}^0$, and 1 are the scalars $\langle 1|T|1\rangle$, $\langle 1|\mathcal{V}|1\rangle$, $\langle 1|G^0|1\rangle$, and 1, respectively.

V. ANALYTIC EXPRESSIONS FOR THE MATRIX ELEMENTS OF G^0

The unperturbed Green's function matrix elements $\langle m|G^0|n\rangle = G^0_{mn}$ between the relevant $2p_z$ carbon orbitals of 2D graphene that enter Eq. (7) are given by

$$G^0_{mn}(\epsilon) = \sum_{k,p} \frac{\langle m|\Phi_{kp}\rangle\langle\Phi_{kp}|n\rangle}{\epsilon + i\eta - \langle\Phi_{kp}|H_0|\Phi_{kp}\rangle}, \tag{8}$$

where $|\Phi_{kp}\rangle$ are the eigenstates of the unperturbed Hamiltonian H_0 of 2D graphene given by Eq. (1), with wave vector k and band index $p = \pm 1$.

We evaluate the diagonal matrix element $\langle 1|G^0|1\rangle = G^0_{11}(\epsilon)$ as follows: For $m = n = 1$ and small ϵ the summand in Eq. (8) is strongly peaked in k-space around the Dirac points. We therefore approximate the sum over the Brillouin zone in Eq. (8) by the sum of integrals over two circles in k-space centered on the two Dirac points K and K', choosing the area of each circle to be equal to half of that of the Brillouin zone. We then evaluate the integrals by linearizing $\langle\Phi_{kp}|H_0|\Phi_{kp}\rangle$ in k about each Dirac point in the standard way, which yields $\langle\Phi_{kp}|H_0|\Phi_{kp}\rangle \approx \pm 3t\tau|k|/2$ where τ is the nearest-neighbor spacing between graphene carbon atoms. This yields[95]

$$G^0_{11}(\epsilon) \approx \frac{\epsilon}{\sqrt{3}\pi t^2}\ln\left(\frac{\epsilon^2}{\sqrt{3}\pi t^2 - \epsilon^2}\right) - i\frac{|\epsilon|}{\sqrt{3}t^2}, \tag{9}$$

For comparison we carried out an exact numerical evaluation of Eq. (8) *without* linearizing $\langle\Phi_{kp}|H_0|\Phi_{kp}\rangle$ or approximating the Brillouin zone or the unperturbed model Hamiltonian $H_0 = -\sum_{\langle n,m\rangle} t(a_n^\dagger a_m + \text{h.c.})$ of 2D graphene or its eigenvalues or eigenfunctions in any way. We found the analytic approximation [Eq. (9)] to agree with our exact numerical results to within a few percent for small values of ϵ. We also found that the accuracy of Eq. (9) can be improved and extended to larger $|\epsilon|$ with the help of empirical correction factors $\alpha(\epsilon) = 1.07(1 + 0.66\,\epsilon^2/t^2)$ and $\beta(\epsilon) = 1 + 0.31\epsilon^2/t^2 + 0.33\,\epsilon^4/t^4$. The resulting expression,

$$G^0_{11}(\epsilon) = \frac{\epsilon\alpha(\epsilon)}{\sqrt{3}\pi t^2}\ln\left(\frac{\epsilon^2}{\sqrt{3}\pi t^2 - \epsilon^2}\right) - i\frac{|\epsilon|\beta(\epsilon)}{\sqrt{3}t^2}, \tag{10}$$

is accurate in the range $|\epsilon|/t \leqslant 0.8$. We note that several less accurate analytic approximations for $G^0_{11}(\epsilon)$ have also been

proposed in the literature.[60,63,66,69,71] The first of these[60] underestimated $G^0_{11}(\epsilon)$ by more than a factor of 2, due in part to the use of an inadequate model of the graphene electronic structure with only a single Dirac cone instead of the two such cones that are centered at the Dirac points K and K' of graphene in reality. The most accurate of them[60,63,66,69,71] is that given by Eq. 37a in Ref. 66 with ϵ replaced by $|\epsilon|$ in the imaginary term. $G^0_{mn}(\epsilon)$ can also be expressed exactly in terms of elliptic integrals that, however, must be evaluated numerically.[96]

The analytic approximation scheme that leads to Eq. (9) is inappropriate for evaluating $G^0_{21}(\epsilon)$ directly because in that case the summand in Eq. (8) is not maximal at the Dirac points K and K' where the linear approximation to $\langle\Phi_{kp}|H_0|\Phi_{kp}\rangle$ is accurate. However an analytic expression for $G^0_{21}(\epsilon)$ that is accurate in the same energy range as Eq. (10) can still be obtained as follows.

We start from the identity

$$\langle 1|(\epsilon + i\eta - H_0)G_0(\epsilon)|1\rangle = 1, \tag{11}$$

from which it follows that

$$(\epsilon + i\eta)\langle 1|G_0(\epsilon)|1\rangle + \sum_{n=2}^{4}\langle 1|(-H_0)|n\rangle\langle n|G_0(\epsilon)|1\rangle = 1. \tag{12}$$

In Eqs. (11) and (12), $|1\rangle$ is the $2p_z$ orbital of a carbon atom and $|n\rangle$ for $n = 2,3,4$ are the $2p_z$ orbitals of its three nearest neighbors. Analysis of Eq. (8) shows that, because of the threefold rotational symmetry of infinite 2D graphene, $\langle 2|G_0(\epsilon)|1\rangle = \langle 3|G_0(\epsilon)|1\rangle = \langle 4|G_0(\epsilon)|1\rangle$. Then, since $\langle 1|(-H_0)|n\rangle = t$ and taking the limit $\eta \to 0$ we obtain from Eq. (12) the exact result that

$$G^0_{21}(\epsilon) \equiv \langle 2|G_0(\epsilon)|1\rangle = \frac{1}{3t} - \frac{\epsilon}{3t}G^0_{11}(\epsilon). \tag{13}$$

It is then straightforward to show also that $G^0_{21}(\epsilon) = G^0_{12}(\epsilon)$. Finally, inserting Eq. (10) into Eq. (13), we obtain

$$G^0_{21}(\epsilon) = \frac{1}{3t} - \frac{\epsilon^2\alpha(\epsilon)}{3\sqrt{3}\pi t^3}\ln\left(\frac{\epsilon^2}{\sqrt{3}\pi t^2 - \epsilon^2}\right) + i\frac{\epsilon|\epsilon|\beta(\epsilon)}{3\sqrt{3}t^3}. \tag{14}$$

We have compared the analytic expression (14) with the results of our exact numerical evaluation of $G^0_{21}(\epsilon)$ and found Eq. (14) to be accurate under the same conditions as Eq. (10), as expected. Previous theoretical work[62,66] has yielded analytic expressions for $G^0_{21}(\epsilon)$ only for the special case $\epsilon = 0$. For that case Eq. (14) reduces to $G^0_{21}(0) = \frac{1}{3t}$, which agrees with the result stated in Ref. 66 but differs in sign from that stated in Ref. 62. It should be noted that the sign of G^0_{21} is not arbitrary; the calculated Dirac point resonance for O adsorbed on graphene is modified significantly if this sign is reversed.

VI. DIRAC POINT RESONANCES OF H, F, OH, AND O ADSORBATES ON GRAPHENE

The strength of scattering associated with a defect is in general proportional to the square modulus of appropriate matrix elements of the T-matrix. Thus the energies ϵ at which resonant scattering by H, F, OH, and O adsorbates should occur are those at which $|\langle m|T|n\rangle|^2$ have maxima. We find these energies to be close to those at which $|1 - \tilde{\mathcal{V}}\tilde{G}^0|^{-2}$ for H, F, and OH or $|\det(1 - \tilde{\mathcal{V}}\tilde{G}^0)|^{-2}$ for O have maxima.

The square moduli of the matrix elements of the T-matrix defined in Sec. IV and calculated using the tight-binding parameters $\gamma_{\alpha j}$ and ϵ_α obtained from extended Hückel theory as is described in Sec. II are shown vs. the electron energy ϵ in Fig. 2. The extended molecular orbitals ψ_α included in these calculations are linear combinations of the atomic valence orbitals of the adsorbed species and the $2s$, $2p_x$, and $2p_y$ valence orbitals of all of the carbon atoms shown in Fig. 1 for the respective adsorbed species. There are 13, 16, 17, and 22 EMOs included in the calculations for H, F, OH, and O, respectively. The overlaps $\sigma_{\alpha j}$ between the EMOs ψ_α and the $2p_z$ orbitals ϕ_j of carbon atoms j to which the adsorbed moieties bond are included in the calculations as is discussed at the end of Sec. II.

For each adsorbed species the T-matrix displays a prominent resonant peak (a double peak for O in Fig. 2) in the vicinity of $\epsilon = 0$, the Dirac point of graphene. The electron energy ϵ_{DR} at which the resonance is centered depends on the adsorbed species; $\epsilon_{DR} = -0.136t, -0.089t, -0.0026t$ for F, OH, and H, respectively. For O there is a narrow peak near $0.112t$ that overlaps a broader peak centered near $0.090t$. The strengths of the F, OH, and broader O resonances (as measured by the area under the resonance curve when plotted on a linear scale) are all comparable. The narrow O resonance is an order

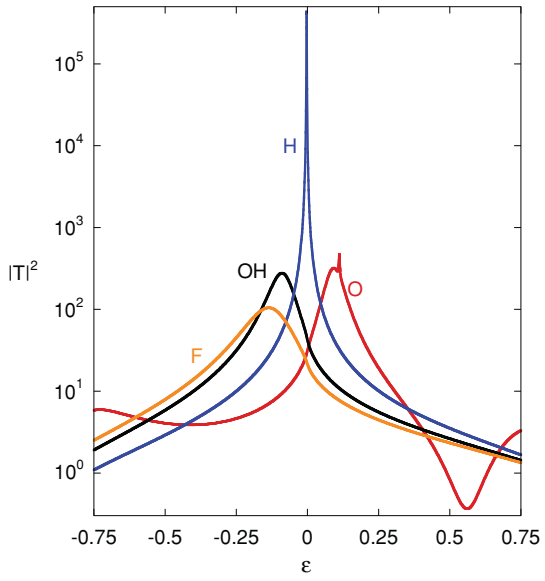

FIG. 2. (Color online) Calculated square modulus of the T-matrix vs. electron energy ϵ for an H, F, or O atom or OH group adsorbed on graphene in the geometries shown in Fig. 1. T and ϵ are in units of $t = 2.7$ eV. The Dirac point of graphene is at $\epsilon = 0$. For H, F, and OH $T = \langle 1|T|1\rangle$. For O the square of the Frobenius norm of the matrix $\langle m|T|n\rangle$ is plotted. The EMOs included in this calculation are linear combinations of the atomic valence orbitals of the adsorbed species and the $2s$, $2p_x$, and $2p_y$ valence orbitals of each of the carbon atoms shown in Fig. 1 for the respective adsorbed species. Thus the local rehybridization of the graphene from the sp^2 to sp^3 bonding is included in the model. The overlaps $\sigma_{\alpha j}$ between the EMOs and the $2p_z$ orbitals of the carbon atoms to which the adsorbed moieties bond are included in the calculations.

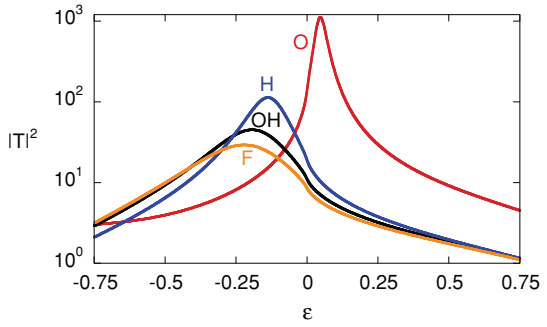

FIG. 3. (Color online) Calculated square modulus of the T-matrix vs. electron energy ϵ for a simpler model of H, F, or O atom or OH group adsorbed on graphene than that used in the calculations presented in Fig. 2: Here only the valence orbitals of the adsorbed species themselves (no carbon orbitals) are included in the EMOs. The parameters ϵ_α and $\gamma_{\alpha j}$ used are from Table II; the molecular orbitals ψ_α are used in the case of OH. The overlaps $\sigma_{\alpha j}$ are also included in the calculation. Notation as in Fig. 2.

of magnitude weaker than these while the H resonance is two orders of magnitude stronger.

For comparison the results of a similar calculation but for a simpler model in which the carbon atom $2s$, $2p_x$, and $2p_y$ valence orbitals are omitted from the EMOs are shown in Fig. 3. In this case $\epsilon_{\rm DR} = -0.222t, -0.194t, -0.138t$, and $0.046t$ for F, OH, H, and O, respectively.[97] Comparing Fig. 2 with Fig. 3, it is evident that the coupling of the adsorbate to the graphene carbon $2s$, $2p_x$, and $2p_y$ valence orbitals (which are involved in the partial rehybridization of the carbon atom to which the adsorbate bonds to the sp^3 electronic structure) can affect adsorbate-induced Dirac point resonances very strongly: It is directly responsible for the H resonance in Fig. 2 being two orders of magnitude stronger than the resonances for F, O, and OH. It is also responsible for the *double* peak structure of the O resonance in Fig. 2 that is absent in Fig. 3. Notice also the *antiresonance* in the O T-matrix near $\epsilon = 0.55t$ in Fig. 2 that is absent in Fig. 3.

The Dirac point resonance energy increases from F to OH to H to O in both models and the sign of the resonance energy for each species (negative for F, OH, and H and positive for O) is the same in both models. However, the coupling of the H adsorbate to the graphene carbon $2s$, $2p_x$, and $2p_y$ valence orbitals results in the H Dirac point resonance being extremely close to the Dirac point of graphene ($\epsilon_{\rm DR} = -0.0026t$) in Fig. 2. As will be seen in Sec. IX this results in the conductances of graphene nanoribbons with hydrogen adsorbates being almost symmetric about the graphene Dirac point (as they are for ribbons with carbon atom vacancies[40]), in marked contrast to the asymmetric conductances for the other adsorbed species.

Finally we find that an accurate description of the Dirac resonance profiles in Fig. 2 (including their energies, widths, and heights) can be obtained by including in the tight-binding Hamiltonian, Eq. (4), relatively small sets of EMOs since some of the EMOs couple only weakly to the graphene π system. The EMO energies ϵ_α and coupling parameters $\gamma_{\alpha j}$ for a minimal tight-binding model Hamiltonian that describes the Dirac point resonance profiles shown in Fig. 2 are presented in Table I.

TABLE I. Minimal set of effective tight-binding parameters ϵ_α and$\gamma_{\alpha j}$ in units of $t = 2.7$ eV for adsorbed H, F, and O atoms and OH on graphene. The EMO energies ϵ_α are measured from the Dirac point energy of graphene. $\pm$ means that $\gamma_{\alpha j}$ has opposite signs for the two carbon atoms to which the O atom bonds.

Adsorbate	ϵ_α	$\gamma_{\alpha j}$
H	−0.0383	2.219
F	−10.862	4.363
	−2.460	1.645
	−0.914	1.180
OH	−8.536	3.203
	−1.820	1.779
	−0.709	1.540
O	−5.356	3.240
	−1.448	±1.000
	−0.373	1.095
	0.130	±0.176
	1.463	1.650

The EMO energy and coupling parameter sets presented in Table I will be used in the more sophisticated version of our transport calculations on graphene nanoribbons that we report in Sec. IX. The values of ϵ_α given in Table I are the energies of EMOs calculated from extended Hückel theory as discussed in Sec. II. However, the values of some of the $\gamma_{\alpha j}$ that are given have been adjusted so that the small set of parameters ϵ_α and $\gamma_{\alpha j}$ given in Table I yields a good fit to the resonance profiles in the energy range $-0.75t < \epsilon < 0.75t$ shown in Fig. 2 without the need to include the overlaps $\sigma_{\alpha j}$ in the calculation.

VII. COMPARISON WITH DENSITY-FUNCTIONAL-THEORY-BASED MODELS OF DIRAC POINT RESONANCES

In the previous attempts to construct tight-binding models of Dirac point resonances for use in transport calculations in graphene, the tight-binding parameters were obtained by fitting the results of *ab initio* density-functional-theory-based electronic structure calculations to very simple tight-binding models. In those models the adsorbed atom or molecule M was described by just a *single* effective orbital energy parameter $\epsilon_{\rm M}$ and a *single* coupling parameter $\gamma_{\rm M}$. For example, $\epsilon_{\rm H} = 0.66t$ and $\gamma_{\rm H} = 0.22t$ were obtained for adsorbed hydrogen and $\epsilon_{\rm OH} = -2.9t$ and $\gamma_{\rm OH} = 2.3t$ were obtained for the adsorbed hydroxyl group in Ref. 64. On the other hand, in Ref. 70 *much smaller* values of the effective orbital energy parameter $\epsilon_{\rm M} \leqslant 0.1t$ were found for a number of covalently bonded adsorbed species, including hydrogen, and $\gamma_{\rm M} \geqslant 2t$ was found for the same species.

That such very different results have been obtained from density-functional-theory-based calculations even for hydrogen, the simplest of all adsorbed species, raises the question whether density functional calculations, although putatively a "first-principles" method, are a sound basis for theoretical studies of the Dirac point resonances of graphene with adsorbates. This demonstrated lack of consistency may be related to the fact that density functional theory, although well suited to calculations of the total ground-state energies of

many condensed matter systems, is known to have important *fundamental* deficiencies as a methodology for electronic structure calculations; for a recent discussion of the relevant physics and a review of the literature the reader is referred to Ref. 50.

As a consequence of these deficiences, for example, density functional calculations underestimate the bandgap of silicon and other semiconductors by as much as a factor of 2. They also yield offsets between the energy levels of molecules adsorbed on silicon and the silicon valence band edge that more sophisticated theories indicate to be in error by as much as 1.4 eV.[98] The latter error is similar in size to the above-mentioned discrepancy between the values of ϵ_H predicted by the density functional theory calculations reported in Refs. 64 and 70 for H adsorbed on graphene.

Because different density-functional-theory-based electronic structure calculations have yielded such different results even for the Dirac point resonance due to hydrogen on graphene, we chose instead to base our electronic structure calculations on the well-known *semiempirical* extended Hückel model of quantum chemistry. The extended Hückel model has been parametrized[72] based on a large body of *experimental* electronic structure data for atoms and molecules and has been used successfully in electronic transport calculations for a variety of molecular systems, as has been outlined in Sec. I. The relative merits of electronic structure calculations based on density functional theory and those based on extended Hückel theory have been discussed in detail in Sec. 4.7 of Ref. 50.

The minimal tight-binding model parameters for the Dirac point resonance due to hydrogen adsorbed on graphene that we derived from extended Hückel theory using the methodology described in Secs. II–VI are given in Table I. They are in excellent agreement with the corresponding density-functional-theory-based results $\epsilon_M \leqslant 0.1t$ and $\gamma_M \geqslant 2t$ stated in Ref. 70 but are not consistent with the density-functional-theory-based results $\epsilon_H = 0.66t$ and $\gamma_H = 0.22t$ reported in Ref. 64.

We find *one*-orbital tight-binding models such as those used in Refs. 64 and 70 not to yield a satisfactory description of Dirac point resonances for the other adsorbed species (F, OH, and O) that we have considered within extended Hückel theory. Therefore comparing our tight-binding models for the Dirac point resonances of those species directly with the corresponding tight-binding parameters that have been derived from density functional theory (as we have done above for the case of adsorbed hydrogen) is not possible. However, we have calculated the local densities of states (LDOSs) associated with the Dirac point resonances within our extended Hückel-based model for these adsorbates and compare them below with the corresponding LDOS features calculated using density functional theory in Ref. 68.

Our calculated LDOSs for graphene with an adsorbed H, F, or O atom or OH group are shown in Fig. 4. The extended Hückel-theory-based model used in these calculations is the same as that used to calculate the square moduli of the T-matrices that are shown in Fig. 2. That is, the EMOs included the calculations are linear combinations of the atomic valence orbitals of the adsorbed species and the $2s$, $2p_x$, and $2p_y$ valence orbitals of each of the carbon atoms shown in Fig. 1 for the respective adsorbed species. Thus the model includes the effects of the local rehybridization of the graphene due to the presence of the adsorbate. The quantities plotted in Fig. 4 are the partial LDOSs defined by $D_n(\epsilon) = -\mathrm{Im}(\langle n|G(\epsilon)|n\rangle)/\pi$, where G is defined by Eq. (5) and $|n\rangle$ represents a $2p_z$ orbital of a carbon atom. The dashed black curves are for graphene carbon atoms to which the adsorbed moieties bond, and the solid red curves are for nearest (carbon) neighbors of those carbon atoms. Note the different energy scale used for the case of H and also that the dashed black curve for H has been scaled up for clarity by a factor of 500. In each plot the Dirac point is at $\epsilon = 0$. The energies at which the peaks of the densities of states occur in Fig. 4 are reasonably close to the energies of the Dirac point resonance peaks for the respective adsorbates in Fig. 2, the largest discrepancy being $\sim$20% for fluorine.

The partial LDOS in Fig. 4 for H, F, and O can be compared with the corresponding density-functional-theory-based results in Figs. 1(c), 1(d), and 5(a) of Ref. 68, respectively. However, some differences between the systems considered should be noted: The results in Fig. 4 are for a single

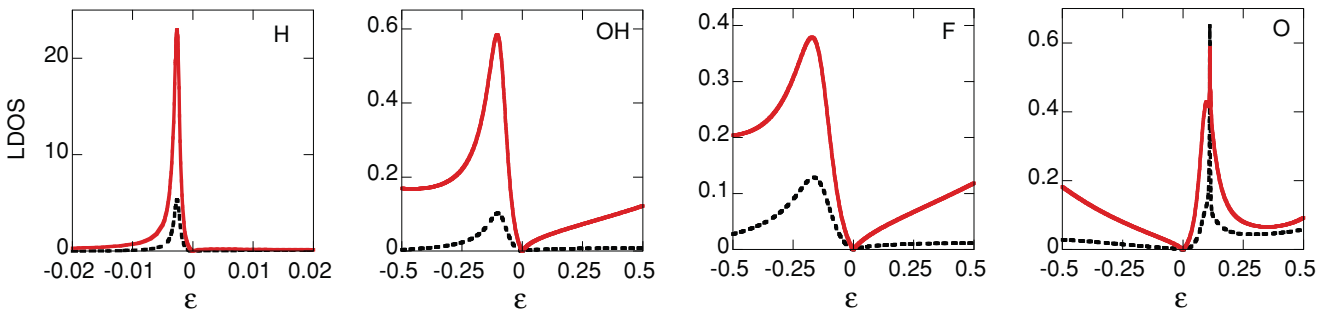

FIG. 4. (Color online) Calculated LDOSs vs. electron energy ϵ for an H, F, or O atom or OH group adsorbed on graphene in the geometries shown in Fig. 1. The LDOS is in units of $1/t$ and ϵ is in units of $t = 2.7$ eV. For F and O atoms and OH the black dashed curves show the LDOS associated with the $2p_z$ orbital of a carbon atom to which the adsorbed moiety bonds. For H the black dashed curve shows the LDOS associated with the $2p_z$ orbital of a carbon atom to which the adsorbed atom bonds multiplied by 500. The red solid curves show the LDOS associated with the $2p_z$ orbital of a carbon atom that is a nearest neighbor of a carbon atom to which the adsorbed moiety bonds. The Dirac point of graphene is at $\epsilon = 0$. The EMOs included in this calculation are linear combinations of the atomic valence orbitals of the adsorbed species and the $2s$, $2p_x$, and $2p_y$ valence orbitals of each of the carbon atoms shown in Fig. 1 for the respective adsorbed species. Thus the local rehybridization of the graphene from the sp^2 to sp^3 bonding is included in the model.

adsorbed atom or molecule on an infinite graphene sheet whereas those in Ref. 68 are for periodic structures with 4×4 graphene supercells each containing an adsorbed moiety. Thus in Ref. 68, in contrast to the present work, the Dirac point resonance is expected to be broadened due to the presence of multiple adsorbed atoms on the graphene. Also, the density of states (DOS) features for H, F, and O in Ref. 68 are located relative to the Fermi energy. The latter may be close to the Dirac point energy but its location relative to the Dirac point energy is not determined *precisely* since in the model systems studied in Ref. 68 there are no very large regions of pristine graphene with no adsorbate where the Dirac point is well defined.

With these caveats, the LDOS for the Dirac point resonance for H in Fig. 4 is consistent with that in Ref. 68, although for the latter the resonance is broader and the partial LDOS on the carbon atom to which the H bonds is not as weak relative to the partial LDOS on its nearest carbon atom neighbors. The LDOS for the fluorine Dirac point resonance in Ref. 68 is also similar to that in Fig. 4, although the LDOS peaks in the latter are somewhat lower in energy relative to the Dirac point than those in the former are relative to the Fermi energy. However, as we have already noted, the precise location of the Fermi level relative to the Dirac point is uncertain in the density-functional-theory-based calculations.

The LDOS for O in Fig. 4 differs markedly from that in Ref. 68: There is no obvious peak in the LDOS in the immediate vicinity of the Fermi energy in the latter case in contrast to the peaks associated with the Dirac point resonance $\sim 0.1t$ above the Dirac point in the former. The reasons for this difference are not clear at present. We note, however, that, as has been discussed above, different density-functional-theory-based calculations[64,70] have yielded very different results even for the Dirac point resonance for adsorbed hydrogen. Furthermore, recent theoretical work[48] has shown even *gross* features of the electronic structures of narrow graphene nanoribbons with high concentrations of adsorbed O at the ribbon edges (including the presence or absence of a large bandgap at the Fermi level) calculated using density functional theory to be sensitive to the precise choice of the exchange-correlation energy functional used in the calculations. While the calculated LDOS for O in Ref. 68 resembles qualitatively that found for a "double impurity" in a simple tight-binding model[68] it should be noted that in that model the double impurity represents *two* atoms that are adsorbed on adjacent carbon atoms and do not interact with each other directly, a situation that is very different than a *single* oxygen atom that bonds to *two* adjacent carbon atoms in its lowest energy configuration in reality and in our extended Hückel-theory-based model.

Given the differing theoretical predictions that we have discussed above, it is evident that experiments probing adsorbate-induced Dirac point resonances in graphene would be of considerable interest.

VIII. MODEL HAMILTONIAN FOR TRANSPORT CALCULATIONS IN GRAPHENE NANORIBBONS

In this section we describe how the tight-binding Hamiltonians developed in the preceding sections for adsorbates on infinite 2D graphene are adapted for calculations of quantum transport in graphene nanoribbons with adsorbates that we consider in the remainder of this paper.

We describe the graphene ribbons by the tight-binding Hamiltonian

$$H = H_\pi + \sum_\alpha \epsilon_\alpha d_\alpha^\dagger d_\alpha + \sum_{\alpha,j} \gamma_{\alpha j}(d_\alpha^\dagger a_j + \text{h.c.}), \quad (15)$$

where

$$H_\pi = -\sum_{\langle i,j\rangle} t_{ij}(a_i^\dagger a_j + \text{h.c.}), \quad (16)$$

t_{ij} is the Hamiltonian matrix element between nearest-neighbor $2p_z$ carbon orbitals of the π-band of the graphene nanoribbon, $a_i^\dagger$ is the creation operator for an electron in $2p_z$ carbon orbital i, and $d_\alpha^\dagger$ creates an electron in an EMO ψ_α that is associated with an adsorbed atom or molecule and has energy ϵ_α. As defined in Sec. II, an EMO is a linear combination of the valence orbitals of the adsorbed atom or molecule and (in the more sophisticated versions of the model) the $2s$, $2p_x$, and $2p_y$ valence orbitals of the graphene carbon atom(s) to which the adsorbate bonds and neighboring graphene carbon atoms. The graphene $2p_z$ orbitals are not included in the EMOs since they are included in the tight-binding Hamiltonian H through H_π. In the present paper we include for simplicity only coupling matrix elements $\gamma_{\alpha j}$ between the EMOs associated with the adorbates and the $2p_z$ valence oribitals of the graphene carbon atoms to which that adsorbed atoms or molecules bond.

In the graphene ribbon π-band Hamiltonian H_π we include nearest-neighbor Hamiltonian matrix elements t_{ij}. For most of these we set $t_{ij} = t = 2.7$ eV, the usual value for tight-binding theories of pristine graphene.[59,88] However, interaction with the H, F, OH, and O adsorbates shifts the carbon atoms to which these moieties bond out of the graphene plane by fractions of an angstrom, perturbing the values of t_{ij} between the carbon atoms to which the adsorbates bond and their neighbors. Although we find the effect of this change in t_{ij} on electron transport in ribbons to be modest (typically less that a 15% difference in the conductance) we include it in the calculations presented in this paper, estimating the modified values of t_{ij} by applying extended Hückel theory to the relaxed geometries of the graphene in the presence of the adsorbates.[99] We do not, however, consider edge reconstruction effects and spin and electron interaction phenomena; these are outside of the scope of the present study.

An important effect associated with the shifting of carbon atoms out of the graphene plane that occurs upon adsorption of H, F, OH, or O is the local partial rehybridization of the graphene from sp^2 to sp^3 bonding. We shall elucidate the role that the rehybridization plays in transport in graphene ribbons by comparing the results of transport calculations for two models:

(i) a simpler model in which the EMOs associated with adsorbed atoms or molecules are approximated by linear combinations of only the valence orbitals of the adsorbed species, and

(ii) a model in which the EMOs are linear combinations of the the valence orbitals of the adsorbed species *and* of the appropriate valence orbitals ($2s$, $2p_x$ and $2p_y$) of the graphene carbon atoms involved in the rehybridization, i.e., the

carbon atoms to which the adsorbate bonds and their nearest neighbors.

For case (ii) the number of EMOs per adsorbed moiety is too large for exact quantum transport calculations to be carried out with the computational resources available to us for ribbons of experimentally relevant sizes and adsorbate concentrations of interest. However, it was found in Sec. VI that reduced sets of between one and five EMOs per adsorbed moiety with suitably adjusted values of $\gamma_{\alpha j}$ are sufficient to provide an accurate description of the Dirac point resonances in graphene induced by H, F, OH, and O adsorbates. These minimal sets (with parameters listed in Table I) will be used in the transport calculations for case (ii) that we present in this paper.

In our transport calculations the adsorbed atoms and molecules are introduced by randomly placing them on the graphene surface. They are characterized by the probability p to find an adsorbed moiety per carbon atom. To convert p to the usual concentration one should scale it by the number of carbon atoms divided by the sample size, 3.8×10^{19} m^{-2}.

In the linear response regime the zero-temperature conductance of the graphene ribbon is given by the Landauer formula[50,100–103]

$$G = \frac{2e^2}{h} \sum_{ji} T_{ji}, \tag{17}$$

where T_{ji} is the transmission coefficient from the subband i in the left lead to the subband j the right lead, at the Fermi energy. For nonzero temperatures,

$$G = -\frac{2e^2}{h} \int_{-\infty}^{\infty} dE\ T(E) \frac{\partial f(E)}{\partial E}, \tag{18}$$

where $T(E) = \sum_{ij} T_{ji}(E)$ and $f(E)$ is the Fermi distribution function. T_{ji} is calculated by the recursive Green's function method; see Ref. 32 for details.

IX. RESULTS

In our transport calculations the ribbon has a width $W =$ 30 nm as in the experiments of Lin *et al.*[3] The adsorbed H, F, OH, or O are assumed to be present only in a finite region of length $L = 500$ nm of the ribbon which is attached at its two ends to semi-infinite leads represented by ideal ribbons of the same width. The edge configuration is taken as armchair in the following. For comparison we also present some results for ribbons with interior carbon atom vacancy defects modeled in the same way as in Ref. 40.

A. Ribbons with H adatoms

1. Atomic geometry and electronic structure

Hydrogen is the simplest adsorbate that bonds covalently to a carbon atom of the graphene lattice. According to the extended Hückel model, the H $1s$ orbital energy locates not far from the Dirac point of graphene, $\epsilon_{H_{1s}} = -0.81t$, and the Hamiltonian matrix element between the hydrogen $1s$ orbital and the carbon $2p_z$ orbital of the closest graphene carbon atom, $\gamma_{H_{1s},C_{2p_z}} = 1.89t$ (see Table II), is nearly twice as large as the Hamiltonian matrix element t between the $2p_z$ orbitals of adjacent carbon atoms. Adsorption of the H atom also results in a modified graphene lattice geometry. In the relaxed geometry, we find significant lifting of the carbon atom directly bound to the H out of the graphene plane by 0.35 Å. This is accompanied by weakening of the $C_{2p_z} - C_{2p_z}$ Hamiltonian matrix element between the C atom to which the H atom binds and its neighbor C atoms to $0.79t$. Since the graphene sheet is no longer planar, partial rehybridization from sp^2 to sp^3 occurs near the adsorbed H atom: The carbon atom to which the H atom binds can be regarded as forming σ bonds with its carbon atom neighbors and with the H atom. The rehybridization of the graphene on adsorption of the H atom and the strong coupling between H adatom and the graphene result in strong scattering of graphene π-band electrons near the adsorbed H atom.

TABLE II. Tight-binding parameters for the adsorbed H, F, O, and OH in units of $t = 2.7$ eV for the simplest model in which the EMOs do not include the carbon $2s$, $2p_x$, and $2p_y$ atomic orbitals. The atomic and molecular orbital energies ϵ_α are measured from the Dirac point of graphene. $\gamma_{\alpha,C_{2p_z}}$ is the Hamiltonian matrix element between the orbital ψ_α of the adsorbate and the $2p_z$ orbital of the nearest graphene C atom. The $\pm$ means that the $\gamma_{\alpha,C_{2p_z}}$ values for the two C atoms to which the O atom bonds have opposite signs. For OH the parameters are given for both the atomic O and H orbitals and the molecular orbitals ψ_α of OH. $\gamma_{C_{2p_z},C_{2p_z}}$ is the Hamiltonian matrix element between the $2p_z$ orbital of the graphene C atom to which the adsorbed moiety bonds and the $2p_z$ orbital of a neighboring C atom.[99] For O the first $\gamma_{C_{2p_z},C_{2p_z}}$ is for the pair of C atoms to which the O bonds while the second is for a C atom to which the O bonds and another nearest C neighbor of that C atom.

adsorbate	ψ_α	ϵ_α	$\gamma_{\alpha,C_{2p_z}}$	$\gamma_{C_{2p_z},C_{2p_z}}$
H	$1s$	-0.81	1.89	0.79
F	$2s$	-10.59	4.70	0.79
	$2p_z$	-2.48	1.45	
OH	$2s^{\mathrm{O}}$	-7.74	4.10	0.73
	$2p_z^{\mathrm{O}}$	-1.26	1.24	
	$1s^{\mathrm{H}}$	-0.81	0.36	
OH	ψ_1	-8.17	3.75	0.73
	ψ_2	-1.64	1.81	
	ψ_3	7.39	1.69	
O	$2s$	-7.74	3.47	0.92
	$2p_z$	-1.26	0.76	0.89
	$2p_x$	-1.26	± 0.80	

2. Conduction in ribbons with H adatoms

In Figs. 5(a) and 5(b) we show the calculated conductance of a graphene nanoribbon with a concentration $p^{\mathrm{H}} = 10^{-4}$ of adsorbed H. In Fig. 5(a) the results are shown for the model that includes in the adsorbate EMO the H $1s$ orbital and the $2s$, $2p_x$, and $2p_y$ orbitals of the carbon atom to which the H binds and its neighboring carbon atoms, the tight-binding parameters used being those given in Table I. This model includes the effect of the local rehybridization of the graphene from sp^2 to sp^3 bonding. For comparison the results for a model in which the adsorbate EMO includes only the H $1s$ orbital (with the parameters given in Table II of the present paper) are shown in Fig. 5(b). The conductances of the same ribbon with no adsorbate but an equal concentration $p = 10^{-4}$ of interior carbon atom vacancies[40] and of an ideal ribbon with no adsorbate or vacancies are also shown. In both models,

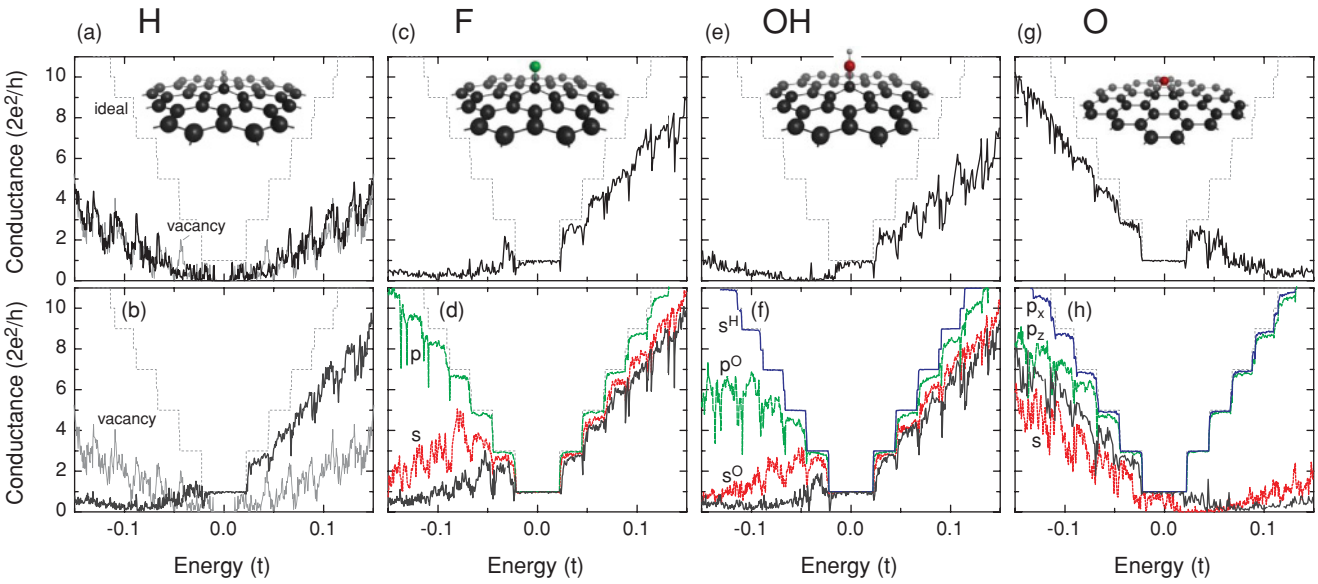

FIG. 5. (Color online) Calculated conductances as a function of the Fermi energy for graphene ribbons with different adsorbed species at a concentration $p = 10^{-4}$. The relaxed geometries of the adsorbed species and nearby graphene atoms are shown in the insets. The dotted gray lines show the conductance of the ideal ribbon without any defects. The solid black lines in (a), (c), (e), and (g) show the calculated conductances of ribbons with H, F, OH, and O adsorbates, respectively, for the model that includes the effects of the adsorbate induced rehybridization of the graphene; the parametrization used is given in Table I. The solid black lines in (b), (d), (f), and (h) show the calculated conductances of ribbons with H, F, OH, and O adsorbates, respectively, for the simpler model that includes only the adsorbate valence orbitals in the EMOs as parametrized in Table II and thus does not include the effects of the rehybridization of the graphene. Red, green, and blue solid lines show the effect on the conductance of the individual orbitals of the adsorbed species as indicated. The gray solid line in (a) and (b) shows the conductance of a ribbon with interior carbon atom vacancies at $p_{vac} = 10^{-4}$. Ribbon width $W = 30$ nm; length $L = 500$ nm; temperature $T = 0$; $t = 2.7$ eV.

even for this low concentration of adsorbed H atoms, the conductance of the ribbon is strongly suppressed relative to that of the ideal ribbon.

The calculated conductance with the rehybridization of the graphene taken into account [the solid black curve in Fig. 5(a)] is strikingly similar both qualitatively and quantitatively to that of the ribbon with the same concentration of carbon atom vacancies (the solid gray curve), whereas the conductance calculated without including rehybridization [the solid black curve in Fig. 5(b)] is qualitatively different.

This is consistent with the idea[67] that the rehybridization should effectively decouple the carbon atom to which the H atom bonds from the graphene π-band, in which case scattering of graphene π-band electrons by an adsorbed H atom would be expected to resemble electron scattering by a carbon atom vacancy. However, this simple picture does not account for the differences between graphene with a H adsorbate and graphene with a F or OH adsorbate: As will be seen below, the conductance characteristics of ribbons with F and OH adsorbates with rehybridization included differ qualitatively from those of ribbons with vacancies and change much less drastically than those for H when rehybridization is included in the model, although the changes in the graphene geometry due to the adsorption of F and OH are very similar to and even slightly larger than for H adsorption.

If the energy scale is broadened (see Fig. 6) an approximately linear increase of the conductance with the absolute value of the energy is found with nearly the same absolute slope at positive and negative energies for ribbons with adsorbed H. Thus on the larger energy scale the conductance of the ribbon is nearly symmetric in the Fermi energy in the presence of adsorbed H as it is in the presence of interior carbon atom

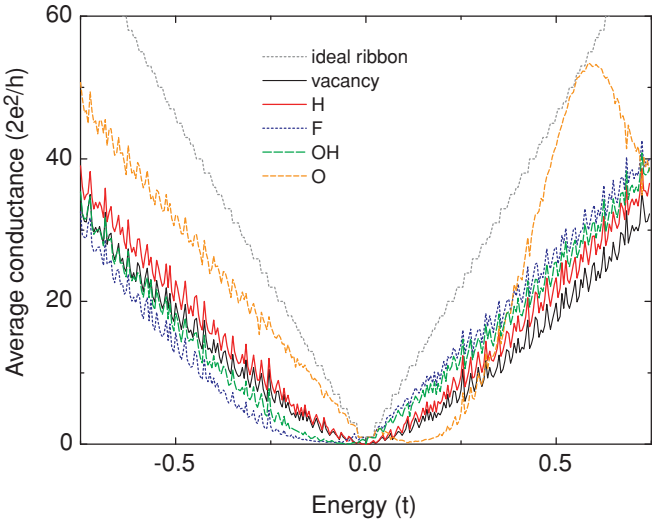

FIG. 6. (Color online) Comparison of the calculated averaged conductances of graphene ribbons with adsorbates (for the model that includes adsorbate-induced rehybridization of the graphene) and interior carbon atom vacancies at a concentration $p = 10^{-4}$ in each case. The averaging in each plot is over 10 arrangements of the positions of the vacancies or adsorbed atoms or molecules. The gray dotted line shows the conductance of the ideal ribbon without any defects.

vacancies. This behavior of the conductance is consistent with experiment.[3]

3. Role of the Dirac point resonance

A clearer understanding of the role of the graphene rehybridization in electron transport can be gained by comparing the conductance plots in Fig. 5(a) (where the rehybridization is included in the model) and Fig. 5(b) (where it is not) with the calculated properties of the Dirac point scattering resonances associated with adsorbed H in the same two models as were used for these transport calculations. The corresponding Dirac point resonances are shown in Figs. 2 and 3, respectively. Ignoring the mesoscopic conductance fluctuations in Fig. 5, it is apparent that including the rebybridization in the transport model results in a shift in the energy of the main conductance minimum from $\sim -0.1t$ in Fig. 5(b) to $\sim 0.0t$ (the Dirac point of graphene) in Fig. 5(a). This matches reasonably well the shift in the energy of the hydrogen Dirac point scattering resonance from $-0.138t$ to $-0.0026t$ that was found upon inclusion of rehybridization in the theory of the H Dirac point resonance in Sec. VI. Thus the locations in energy of the conductance minima for the two models agree quite well with the energies at which the Dirac point resonances of H occur in the models. This is reasonable since strong resonant electron scattering near a particular energy is expected to suppress electron transport near that energy. As will be seen below there is similar agreement between the Dirac point resonance energies and the energies at which the nanoribbon conductance minima occur for the other adsorbates that we study in this article.

A notable feature of the conductance calculated for the nanoribbons with adsorbed hydrogen in the model that does *not* include the graphene rehybridization [Fig. 5(b)] is that in this case the conductance is affected only weakly by the presence of adsorbate when only the lowest nanoribbon subband is populated with electrons. That is, the conductance of the ribbon with the H adsorbate in Fig. 5(b) near the Dirac point is very close to $2e^2/h$, the conductance of the pristine ribbon in the same energy range. This remarkable robustness of transport in the first subband is due to that subband's unique scattering properties arising from the nature of the unconfined electron wave function in graphene.[25,35] Upon inclusion of the graphene rehybridization in our model we found in Sec. VI that in addition to the Dirac point scattering resonance for the H adsorbate shifting to an energy very close to the graphene Dirac point the resonance also becomes stronger by approximately two orders of magnitude. This is sufficient to override the relative robustness of transport in the first graphene nanoribbon subband against scattering so that, unlike in Fig. 5(b), the conductance close to the Dirac point (zero energy) in Fig. 5(a) for the ribbon with the H adsorbate is very strongly suppressed relative to that for the ideal ribbon.

4. Adsorbed H atoms and the density of states

The presence of the adsorbate leads to electron localization at the adsorbed atom or molecule as well as at the nearby carbon atoms. Figure 7(a) shows the LDOS for a ribbon with H adatoms averaged over atoms at different locations. Electron localization is most pronounced for energies near the Dirac point, where the conductance is suppressed most strongly due to resonant backscattering of electrons. Localization is much stronger at the H adatom (including its EMOs) than at the $2p_z$ orbital of the carbon atom to which the H binds. The LDOS for that carbon $2p_z$ orbital is smaller by three orders of magnitude than for the H atom. For this reason it is indistinguishable from the horizontal axis in Fig. 7(a). The carbon atoms adjacent to that carbon atom belong to the other graphene sublattice and exhibit an LDOS as large as that at the H. Strong electron localization is known to occur in graphene near carbon atom

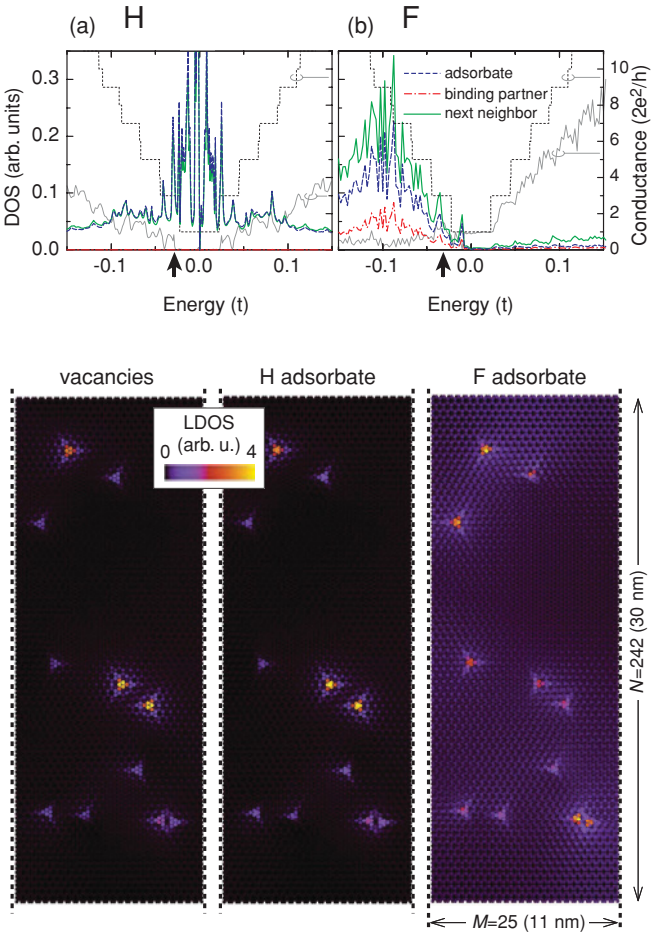

FIG. 7. (Color online) LDOSs averaged over 50 adatoms located at different places in the ribbon vs. electron energy for a ribbon with adsorbed (a) H and (b) F atoms. Adsorbate-induced rehybridization of the graphene is included. The LDOS is shown in red for the $2p_z$ orbital of the C atom to which the adsorbed atom bonds and in green for the $2p_z$ orbital of a C atom neighbor of that C atom. The total LDOS on the EMOs associated with the adsorbed atom (including the contributions of the non-π orbitals of the nearby C atoms) is shown in blue. The dotted and solid gray lines show the conductances of the ideal ribbon and the ribbon with H or F adatoms, respectively. Arrows mark the energy chosen for computation of the LDOS in the bottom panels. The latter are for 15×30 nm^2 fragments of ribbons with interior vacancy defects (left), H adatoms (middle), and F adatoms (right) located at the same places. In the middle and right panels the LDOS for the adsorbate EMOs is combined with the graphene LDOS. For the chosen energy ($-0.03t$) the missing carbon atoms give rise to very similar electron localization close to the defects as the presence of the H adatoms while the LDOS for F is noticeably different.

vacancies.[33,38,59] The lower left and middle panels in Fig. 7 show the LDOSs for two representative graphene ribbons with interior vacancies and H adatoms, with these defects located at corresponding sites in the two ribbons. For the chosen energy $-0.03t$ electrons localize strongly near defects of both types. The C_3 point symmetry of the graphene lattice about the defect sites is clearly visible in the LDOS in the vicinity of each defect. We find the LDOS to decay according to the power law $1/r$ (not shown in Fig. 7) for both defect types, although individual defects may exhibit differing LDOS amplitudes. This power-law decay is consistent with the results of other studies.[67,104]

B. Ribbons with F adatoms

The fluorine adatom bonds covalently to a carbon atom of the graphene lattice and has two valence orbitals ($2s$ and $2p_z$) that scatter graphene π electrons. In the simplest tight-binding model that ignores rehybridization of the graphene, these two orbitals represent two independent channels for electron scattering and their contributions to the scattering are additive (for a single adatom). However, the $2s$ and $2p_z$ orbitals of the F do not contribute equally: The $2s$ orbital couples more strongly to the carbon $2p_z$ orbital since it has the larger value of $|\gamma_{\alpha,C_{2p_z}}|$, as can be seen in Table II. It therefore has the most influence on the electron transport in the graphene ribbon. The coupling of the $2p_z$ orbital is much weaker and has a much smaller effect on the conductance; see Fig. 5(d).

The Dirac point resonance energy for F on graphene was found in Sec. VI to be $-0.136t$ in the model that includes rehybridization and $-0.222t$ in the model that does not. Thus, while the effect of rehybridization of the graphene on the Dirac point resonance of F is important, it is not as drastic as in the case of H. However, as in the case of adsorbed H, these Dirac point resonance energies for F agree well with the energies at which the calculated conductances of ribbons with adsorbed F are most strongly suppressed in both models, as can be seen in Figs. 5(c) and 5(d) and Fig. 6.

In contrast to the case of the H adsorbate, the conductance is affected only weakly by the presence of the F adsorbate when only the lowest nanoribbon subband is populated with electrons for *both* models at the adsorbate concentrations in Figs. 5(c) and 5(d). This is because (unlike for H) the Dirac point resonances for F are offset significantly in energy from the Dirac point in *both* models.

The calculated LDOS for the F adsorbate for the model that includes the rehybridization of the graphene is shown in Fig. 7(b) for the EMOs asociated with the F adsorbate in blue and for the $2p_z$ orbitals of the C atom to which the F binds (red) and its C neighbor (green). In each case the LDOS is strongest around the energy of the F Dirac point resonance. As for H, the LDOS for F is weaker on the $2p_z$ orbitals of the C atom to which the F binds than either on the neighboring C atoms or on the EMOs of the F adsorbate. The spatial map of the LDOS for F shown in the lower-right panel of Fig. 7 is qualitatively similar to that for H and for vacancies, but the particular defect sites showing the strongest LDOS at a given energy are in some cases different for the F.

Notice also that in Fig. 7(b) that there are peaks in the DOS at positive energies near subband edge energies that match dips in the conductance, which is also plotted for comparison. These conductance dips are due to enhanced electron backscattering due to the greater availability of final states for the scattering process at energies with the higher density of subband states, as is discussed in Ref. 40.

C. Ribbons with adsorbed OH groups

The OH molecule is another monovalent adsorbate with many properties similar to F adatoms. In the relaxed geometry the O bonds covalently to a C atom (top site bonding) and the OH chain stands upright relative to the graphene plane, features found also in Refs. 64 and 68. As is seen in Fig. 5(f), the $2s$ and $2p_z$ O orbitals affect electron conduction through the graphene ribbons similarly to $2s$ and $2p_z$ orbitals of F [see Fig. 5(d)], although for O the orbitals scatter electrons somewhat more strongly. The H $1s$ orbital in the OH molecule has much less influence because of its large distance from the C and small overlap with the $2p_z$ C orbital. The total effect of OH adsorbed molecules on the conductance through the graphene ribbon is qualitatively and quantitatively similar to that of F; see also Fig. 6.

The Dirac point resonance energy for OH on graphene was found in Sec. VI to be $-0.089t$ in the model that includes rehybridization and $-0.194t$ in the model that does not. These numbers again agree reasonably well with the energies at which the conductances of ribbons with adsorbed OH is strongly suppressed. The Dirac point resonances for OH occur at energies intermediate between those for H and F in each model and the same is true of the energies at which the strongest suppression of the calculated conductance is seen in Figs. 5 and 6.

As in the case of the F adsorbate, the conductance is affected only weakly by the presence of the OH adsorbate when only the lowest nanoribbon subband is populated with electrons for both models at the adsorbate concentrations in Figs. 5(e) and 5(f), for the same reasons.

D. Ribbons with O adatoms

Oxygen is a divalent adsorbate that binds simultaneously to two neighboring carbon atoms (a bridge site). This leads to substantial rehybridization of the bonding associated with these two carbons that belong to different graphene sublattices. This, in turn, leads to strong electron scattering and suppression of electron conduction through the ribbon.

The calculated conductance vs. energy characteristics for ribbons with adsorbed O are shown in Figs. 5(g) and 6 for the model that includes rehybridization of the graphene and in Fig. 5(h) for the model that does not. The O orbitals affect conduction differently: The O $2s$ orbital produces strong suppression of the conductance at positive energies, but the $2p_z$ orbital suppresses the conductance much less and this occurs mainly at negative energies. The effect of the O $2p_x$ orbital is weaker still. The resulting low conductance at positive energies is a consequence in part of the O adsorbate binding to two carbon atoms belonging to two graphene sublattices unlike the F and OH that bind to a single C atom and exhibit low conductance at negative energies. We note, however, that in general the sign of the energy at which low conductance due to adsorbate scattering occurs depends not only on the

number of C atoms to which the adsorbate binds but also on the values of the model tight-binding parameters ϵ_α and $\gamma_{\alpha j}$. For example, if the absolute values of $\gamma_{\alpha j}$ were substantially smaller than our estimate the low conductance region for O would be at *negative* energies relative to the Dirac point of the ribbon.

As for the other adsorbates discussed above, both the sign and magnitude of the energy at which the conductance of the ribbon with the O adsorbate is suppressed agree well with the energies at which the Dirac point resonances for the O adsorbate were found to occur in Sec. VI, i.e., $0.112t$ and $0.090t$ in the model that includes the graphene rehybridization and $0.046t$ for that which does not.

Another striking feature of Fig. 6 is the prominent conductance maximum for the ribbon with the O adsorbate at energies near $0.55t$. The energy at which the conductance maximum occurs coincides with the energy of the antiresonance (i.e., deep minimum) of the norm of the T-matrix (that describes scattering of graphene electrons due to an adsorbed O atom) that was found in Sec. VI in the model that includes the O adsorbate-induced rehybridization of the graphene.

Since weak electron scattering is normally associated with high conductance, this match between the conductance maximum and the T-matrix antiresonance is intuitively reasonable. It demonstrates once again the close relationship between the T-matrix theory of Secs. IV and VI and transport in graphene ribbons with chemisorbed species that has already been illustrated by the agreement found above between the electron energies at which T-matrix resonances and strong suppression of the ribbon conductances occur.

E. Conductance asymmetry relative to the Dirac point of graphene

In Sec. VI we found the Dirac point resonances for F, OH, and O to be offset in energy from the Dirac point of graphene and in Secs. IX B, IX C, and IX D we showed the electron Fermi energies at which the lowest conductances of ribbons with these adsorbates occur to be offset from the Dirac point of graphene similarly.

Such asymmetric conduction relative to the Dirac point has been discussed in Ref. 64 for the case of infinite 2D graphene. Suppression of the conductivity on one side of the Dirac point with only a weak effect on conduction on the other was explained by a local energy-dependent scattering potential due to the adsorbate.[64] Over a range of energies the conductivity was found to be small while rising linearly outside that range. Qualitatively similar results for 2D graphene were subsequently reported by others.[70,71] A transport gap around the impurity resonance energy had also been predicted earlier for a generic model of infinite 2D graphene with point defects[60] although this prediction was not supported by transport calculations.[60]

This behavior resembles our results for the conductance in the graphene ribbons with F, OH, and O adsorbates but with a qualitative difference: As will be discussed in Sec. IX F, at moderately low temperatures the graphene ribbons exhibit quantized conductance steps superposed on the otherwise linearly rising conductance due to enhanced electron backscattering at the edges of the subbands of the ribbon.

F. Conductance quantization

In the experimental study of Lin *et al.*[3] conductance quantization in the form of conductance steps of equal height was observed in graphene nanoribbon samples with conductances much smaller than $2e^2/h$ in a range of moderately low temperatures as a gate voltage applied to the sample was varied. In a previous paper[40] we showed theoretically that conductance quantization of this kind should occur in graphene nanoribbons with interior carbon atom vacancies even if comparable amounts of other defects such as edge disorder and long-range potentials due to charged defects are also present. However, because of the sample preparation techniques used by Lin *et al.*[3] adsorbed H may well have been present in their samples.

As we have already noted in Sec. IX A 2 [and as is demonstrated very clearly in Fig. 5(a)] the calculated zero-temperature conductance of graphene ribbons with adsorbed H atoms is very similar both qualitatively and quantitatively to that of the ribbon with the same concentration of carbon atom vacancies for the simple model of carbon vacancies considered in Ref. 40. In particular, the properties of the conductance characteristics of ribbons with vacancies that have been shown[40] to give rise to conductance quantization of the kind observed by Lin *et al.*[3] are also exhibited by the conductance characteristic of the ribbon with H adatoms in Fig. 5(a). These properties are as follows:

(i) Pronounced sample-specific conductance fluctuations that are manifestation of quantum interference.[40]

(ii) If the conductance fluctuations are ignored, the conductance is seen to scale down uniformly overall due to scattering by the adsorbate, i.e., in a similar way for all subbands.

(iii) The conductance shows a pronounced dip whenever a new subband becomes available for electron propagation. As is discussed in Ref. 40, this is because of enhanced electron backscattering by the defects at subband edges.

Because of these three properties, we expect graphene nanoribbons with adsorbed H to exhibit equally spaced conductance steps similar to those observed experimentally by Lin *et al.*[3] for the same reasons and under the similar conditions (discussed in Ref. 40) as do graphene nanoribbons with carbon atom vacancies. That is, conductance steps of equal height should be observed even in samples with sufficiently high adsorbate concentrations for the ribbons to have conductances much smaller than $2e^2/h$, the conductance steps should break up into random conductance fluctuations as the temperature approaches 0 K, and the conductance steps should become completely smeared out by thermal broadening at temperatures substantially larger than the subband spacing of the ribbons. This is indeed seen in Fig. 8, where we show the calculated conductance of a ribbon with H adatoms at different temperatures: Regular conductance features are seen at 80 K in Fig. 8(b). They break up into universal conductance fluctuations at 0 K in Fig. 8(a), and are completely smeared out thermally at 300 K in Fig. 8(c).

Thus electron scattering due to a low concentration of H atoms adsorbed on the graphene nanoribbons in our model that takes into account the adsorbate-induced rehybridization of the graphene provides an alternative and equally satisfactory

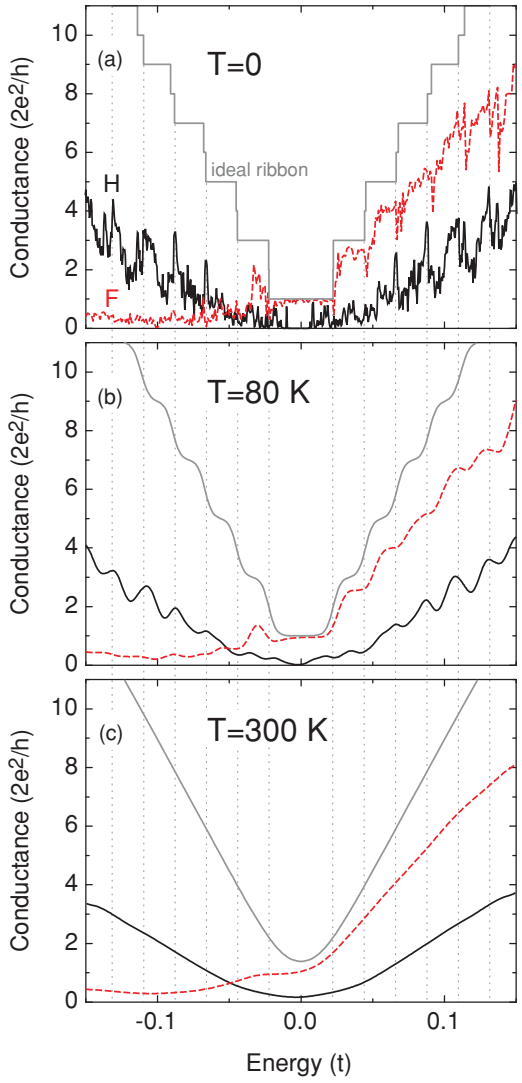

FIG. 8. (Color online) The calculated conductances of ideal graphene ribbons with no adsorbate (solid gray) with H adatoms (solid black) and with F adatoms (dashed red). The temperature is 0, 80, and 300 K in (a), (b), and (c) respectively. Adatom concentrations are $p = 10^{-4}$, as in Fig. 5. Adsorbate induced graphene rehybridization is included in the model. Ribbon width $W = 30$ nm, length $L = 500$ nm, $t = 2.7$ eV.

explanation of the conductance quantization observed by Lin *et al.*[3] to that[40] provided by electron scattering by carbon atom vacancies in the interior of the ribbon.

It is also possible that adsorbed F, OH, and O were present in the samples of Lin *et al.*[3] The three properties, (i), (ii), and (iii), are also shared by ribbons with F, OH, and O adsorbates for positive, positive, and negative energies respectively, as can be seen in Fig. 5(c), 5(e), and 5(g). {Notice also the DOS maxima at subband edges that are responsible[40] for enhanced electron backscattering and hence for a conductance dip whenever the electron Fermi level crosses a subband edge [i.e., property (iii) above] that are clearly visible at positive energies in Fig. 7(b)}. Therefore, conductance quantization of the kind observed by Lin *et al.*[3] should also occur under appropriate conditions for *some* ranges of the gate voltage in graphene ribbons with adsorbed F, OH, and O. Theoretical results for H and F adatoms at various temperatures are shown in Fig. 8. Note that the nearly perfect transmission of electrons in the first subband through the ribbons with F, OH, and O seen in Figs. 5 and 7 is specific to armchair ribbons of particular widths[17] that are metallic and does not occur for insulating ribbons. However, unlike for adsorbed H, for adsorbed F, OH, and O, the Dirac point has a distinctive signature in the calculated conductance that does not coincide with the conductance minimum that is due to the scattering resonance(s) associated with the adsorbate. Such a signature is not evident in the experimental data of Lin *et al.*[3]

In the experimental data of Lin *et al.*[3] there is an offset of about 3 V between the gate voltage at which the conductance minimum occurs and zero gate voltage. The offsets between the energies at which the conductance minima occur in our calculations and the Dirac point energy for F, OH, and O are all smaller than 0.3 eV, the largest being for the F adsorbate. However, we expect other mechanisms such as charged impurities in the insulating spacer between the ribbon and gate electrode or contact potentials between the spacer and gate and/or between the spacer and ribbon to contribute significantly to the the experimentally observed gate voltage at which the conductance minimum occurs.

G. Adsorbate-induced renormalization of the Dirac point and subband edge energies

We note that while for F, OH, and O the conductance minimum is displaced in energy from the Dirac point of the pristine ribbon, this should *not* be interpreted as a shift of the Dirac point of the ribbon due to interaction with the adsorbate;[105] it arises almost entirely from suppression of the conductance by enhanced electron scattering near the conductance minimum.

The actual shift of the Dirac point energy (and subband edge energies) of the ribbon due to interaction of the ribbon with the adsorbate is much smaller and can be estimated perturbatively as follows: If we consider the coupling term $H_c = \sum_{\alpha,j} \gamma_{\alpha j}(d_\alpha^\dagger a_j + \text{h.c.})$ between the adsorbate and the π states the ribbon in the tight-binding Hamiltonian, Eq. (15), as a perturbation, then in second-order perturbation theory this coupling implies a shift Δ_{ks} in the energy of the subband state $|ks\rangle$ given by

$$\Delta_{ks} = \sum_{\alpha,j} |\langle \psi_{\alpha j}|H_c|ks\rangle|^2/(\epsilon_{ks} - \epsilon_\alpha), \tag{19}$$

where ϵ_{ks} is the unperturbed energy of state $|ks\rangle$. For states $|ks\rangle$ that are much closer in energy to the Dirac point of the ribbon than are the orbital energies ϵ_α of the adsorbate we can approximate $\epsilon_{ks} - \epsilon_\alpha \sim -\epsilon_\alpha$ in the denominator of Eq. (19). For OH and F adsorbates that bind to the graphene over a single C atom and assuming that they are randomly distributed over the ribbon we can on average approximate $|\langle \psi_{\alpha j}|H_c|ks\rangle|^2$ by $|\gamma_{\alpha j}|^2/N$, where N is the number of carbon atoms in the ribbon. With these approximations Eq. (19) becomes

$$\Delta_{ks} \sim -p \sum_\alpha |\gamma_{\alpha j}|^2/\epsilon_\alpha, \tag{20}$$

where p is the concentration of the adsorbate and the sum is over the extended molecular orbitals of a single adsorbed atom or molecule. Inserting $p = 10^{-4}$ and the values of $\gamma_{\alpha j}$

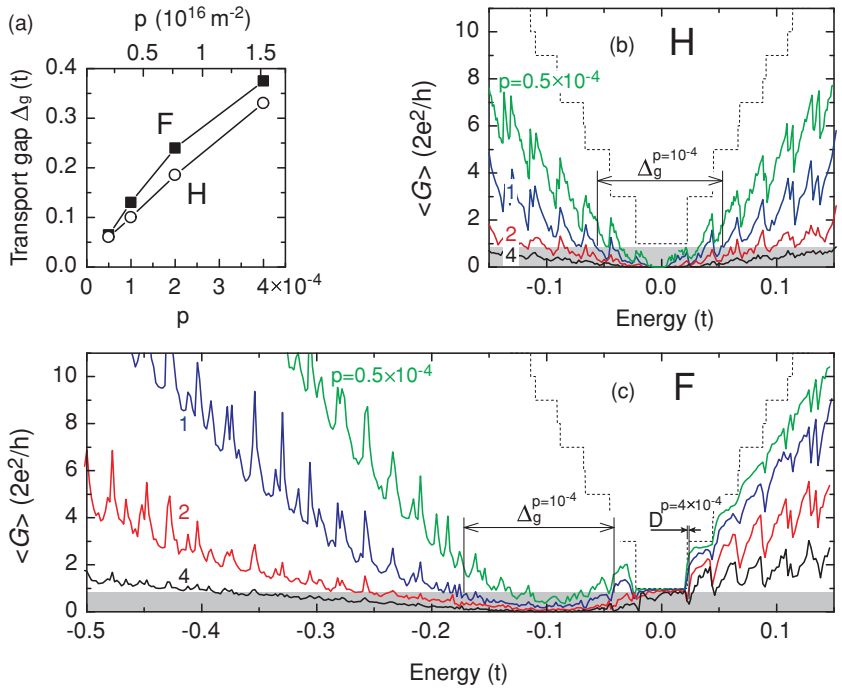

FIG. 9. (Color online) The averaged conductances of graphene ribbons with different concentrations p of adsorbed atoms of (b) H and (c) F averaged over different locations of the adsorbed atoms. The results for $p = 0.5 \times 10^{-4}, 1 \times 10^{-4}, 2 \times 10^{-4}$, and 4×10^{-4} are shown in green, blue, red, and black, respectively. The averaging in each plot is over 10 arrangements of the positions of the adsorbed atoms. The transport gap Δ_g is estimated as the energy interval where $G < 0.9 \times 2e^2/h$. (a) Δ_g increases approximately linearly with p at low p. $D \sim 1.5 \times 10^{-3} t$ in (c) is the offset between the second subband edge for the ideal ribbon with no adsorbate and the center of the conductance dip due to enhanced electron backscattering when the (renormalized) edge of the second ribbon subband crosses the electron Fermi level in the ribbon with a concentration $p = 4 \times 10^{-4}$ of adsorbed F atoms; see the last paragraph of Sec. IX G. Note that $p = 10^{-4}$ corresponds to 3.8×10^{15} adsorbed atoms per square meter. $t = 2.7$ eV.

and ϵ_α from Table I into Eq. (20) we find $\Delta_{ks} \sim 4.4 \times 10^{-4} t$ and $6.3 \times 10^{-4} t$ for F and OH, respectively. These shifts are very small, justifying our use of perturbation theory and demonstrating that the shift of the Dirac point energy due to this mechanism is very small for the adsorbate concentrations considered in this article.

Despite its small size, the energy shift Δ_{ks} has a clear signature in the results of our transport calculations: As we have discussed in Ref. 40 and in the preceding subsections of Sec. IX of the present paper, the conductance of a ribbon with disorder (including that due to randomly located adsorbed moieties) shows a pronounced dip whenever a new subband becomes available for electron propagation due to enhanced electron backscattering by the defects at subband edge energies. Given that the interaction between the ribbon and adsorbate renormalizes the subband edge energies by the amount Δ_{ks} it is to be expected that the energies at which the conductance dips due to scattering by an adsorbate occur should be offset from the subband edge energies of the *pristine* ribbon also by approximately Δ_{ks}. This is indeed what we find. For example, for F adatoms on a ribbon at a concentration $p = 4 \times 10^{-4}$, Eq. (20) yields $\Delta_{ks} = \sim 1.8 \times 10^{-3} t$ which agrees reasonably well with the displacement $D \sim 1.5 \times 10^{-3} t$ of the center of the conductance dip from the second subband edge of the pristine graphene ribbon that is seen for the $p = 4 \times 10^{-4}$ F adsorbate in Fig. 9(c).

H. The transport gaps and their dependence on adatom concentration

Figure 9 shows the conductances of graphene ribbons with different concentration of H and F adatoms. As the adsorbate concentration increases the conductance decreases and a wider transport gap in which the ribbon is effectively an insulator opens centered near the Dirac point for H and at negative energies for adsorbed F. The width Δ_g of the transport gap (that we define arbitrarily as the energy range where the ribbon conductance is less than $0.9 \times 2e^2/h$) grows linearly with the adatom concentration at low concentrations. It worth noting that Δ_g does not depend on the ribbon width, which rules out adsorbate impurities as the principal source of the transport gap in the experiment in Ref. 1.

Transport gaps have been discussed previously in Ref. 106 for graphene with uncompensated vacancies. A $\Delta_g \sim \sqrt{p}$ dependence was found over a wide range of defect concentrations $0 < p < 0.2$. Note, however, that for vacancies randomly distributed over the two sublattices no transport gap was found in Ref. 106. Transport gaps have also been predicted for graphene ribbons substitutionally doped with boron;[49] however, whether the predicted transport gaps are related to Dirac point resonances was not discussed.[49]

X. DISCUSSION

In this paper we have formulated a tight-binding theory of the Dirac point resonances due to adsorbed atoms and molecules on graphene based on the standard tight-binding model of the graphene π-band electronic structure and the extended Hückel model of the adsorbate and the adsorbate-induced local sp^3 rehybridization of the graphene. We generalized previous theories of the effective Hamiltonians of graphene with impurities to the case of adsorbate species with multiple extended molecular orbitals and bonding to more than one graphene carbon atom, and obtained accurate analytic expressions for the Green's function matrix elements that enter the T-matrix theory of Dirac point resonances. This generalization makes the extended Hückel model (and potentially other tight-binding models as well) into a powerful tool for studying the Dirac point resonances induced by many different adsorbates on graphene. Furthermore this theory makes it practical to carry out sophisticated electronic quantum transport calculations for graphene nanoribbons tens of nanometers wide (such as are being realized in present-day

experimental studies) with adsorbates covalently bonded to the ribbon. We applied the above theoretical approach to H, F, OH, and O adsorbates on graphene whose relaxed geometries we calculated with *ab initio* density functional theory. For each of these adsorbates we found a strong scattering resonance near the Dirac point of graphene, the strongest by far being for the H adsorbate. Treating the valence orbitals of the adsorbed species and the $2s$, $2p_x$, and $2p_y$ valence orbitals of the nearby carbon atoms theoretically in a unified way was necessary in order to obtain reliable results. We also extracted from these calculations a minimal set of tight-binding parameters that make it possible to efficiently model adsorbate-induced electron scattering and its effect on electron transport in graphene and graphene nanostructures.

In particular, the minimal tight-binding models that we developed make it possible to model the effect of adsorbates on transport in graphene nanoribbons tens of nanometers wide and hundreds of nanometers long that are at present being realized experimentally. We have presented realistic electronic quantum transport calculations for such nanoribbons with adsorbed H, F, OH, and O. As well as the carbon π-band electronic structure of the graphene nanoribbons our theory includes the effects of the local partial rehybridization of the graphene ribbon from the sp^2 to sp^3 electronic structure that occurs when H, F, OH, or O bonds covalently to the ribbon. This is necessary in order for the model to describe correctly the scattering resonances that are induced in the graphene ribbons near the Dirac point by the presence of these adsorbates. We find that these Dirac point resonances play a dominant role in quantum transport in ribbons with these adsorbates: Even at low adsorbate concentrations of 10^{-4} adsorbed atoms or molecules per carbon atom, in the ribbons that we study the conductance of the ribbon is strongly suppressed and a transport gap is formed for electron Fermi energies in the vicinity of the energy of the resonance. For the H adsorbate this transport gap is centered very close to the Dirac point energy of the ribbon (as it is for ribbons with interior carbon atom vacancies) while for F and OH it is centered below the Dirac point and for O it is centered above the Dirac point. These predictions can be tested experimentally by tuning the position of the Fermi level in the ribbon relative to its Dirac point by means of a variable applied gate voltage. For each of these adsorbed species we find a pronounced dip in the low-temperature conductance of the ribbon when the electron Fermi level crosses the edge of an electronic subband of the ribbon due to enhanced electron backscattering, and the conductance to be suppressed equally on average in every subband. This implies that graphene nanoribbons with H, F, OH, and O adsorbates and conductances even a few orders of magnitude smaller than $2e^2/h$ should (for appropriate ranges of a back gate voltage) exhibit equally spaced conductance steps at moderately low tempertaures, similar to those that have been observed by Lin *et al.*[3] experimentally and that have recently been predicted theoretically[40] for graphene nanoribbons with interior carbon atom vacancies.

Experiments testing these predictions by observing the Dirac point resonances in lateral transport through well-characterized graphene nanoribbons with H, F, OH, and O adsorbates intentionally deposited at known concentrations would be of interest. Vertical transport measurements directed at detecting the Dirac point resonances and measuring the energies at which they occur more directly with the help of scanning tunneling spectroscopy of atoms and molecules adsorbed on graphene and graphene ribbons would also be interesting, especially in view of the often-conflicting predictions of the values of some of these energies that have been made by various theory groups.

ACKNOWLEDGMENTS

We thank A. Saffarzadeh for his helpful comments. This work was supported by NSERC, CIFAR, and WestGrid.

*Canadian Institute for Advanced Research, Nanoelectronics Program.

[1] M. Y. Han, B. Özyilmaz, Y. Zhang, and P. Kim, Phys. Rev. Lett. **98**, 206805 (2007).

[2] Z. Chen, Y.-M. Lin, M. J. Rooks,and Ph. Avouris, Physica E **40**, 228 (2007).

[3] Yu-Ming Lin, V. Perebeinos, Zhihong Chen, and Ph. Avouris, Phys. Rev. B **78**, 161409(R) (2008).

[4] X. Li, X. Wang, L. Zhang, S. Lee, and H. Dai, Science **319**, 1229 (2008).

[5] X. Wang, Y. Ouyang, X. Li, H. Wang, J. Guo, and H. Dai, Phys. Rev. Lett. **100**, 206803 (2008).

[6] F. Molitor, A. Jacobsen, C. Stampfer, J. Güttinger, T. Ihn, and K. Ensslin, Phys. Rev. B **79**, 075426 (2009).

[7] C. Stampfer, J. Güttinger, S. Hellmüller, F. Molitor, K. Ensslin, and T. Ihn, Phys. Rev. Lett. **102**, 056403 (2009).

[8] P. Koskinen, S. Malola, and H. Häkkinen, Phys. Rev. B **80**, 073401 (2009).

[9] L. Jiao, L. Zhang, X. Wang, G. Diankov, and H. Dai, Nature (London) **458**, 87 (2009).

[10] K. Todd, H.-T. Chou, S. Amasha, and D. Goldhaber-Gordon, Nano Lett. **9**, 416 (2009).

[11] D. V. Kosynkin, A. L. Higginbotham, A. Sinitskii, J. R. Lomeda, A. Dimiev, B. K. Price, and J. M. Tour, Nature (London) **458**, 872 (2009).

[12] M. Y. Han, J. C. Brant, and P. Kim, Phys. Rev. Lett. **104**, 056801 (2010).

[13] P. Gallagher, K. Todd, and D. Goldhaber-Gordon, Phys. Rev. B **81**, 115409 (2010).

[14] J. B. Oostinga, B. Sacépé, M. F. Craciun, and A. F. Morpurgo, Phys. Rev. B **81**, 193408 (2010).

[15] L. Jiao, X. Wang, G. Diankov, H. Wang, and H. Dai, Nature Nanotechnol. **5**, 321 (2010).

[16] J. Cai, P. Ruffieux, R. Jaafar, M. Bieri, T. Braun, S. Blankenburg, M. Muoth, A. P. Seitsonen, M. Saleh, X. Feng, K. Müllen, and R. Fasel, Nature (London) **466**, 470 (2010).

[17]K. Nakada, M. Fujita, G. Dresselhaus, and M. S. Dresselhaus, Phys. Rev. B **54**, 17954 (1996).
[18]K. Wakabayashi, Phys. Rev. B **64**, 125428 (2001).
[19]T. Hikihara, X. Hu, H.-H. Lin, and C.-Y. Mou, Phys. Rev. B **68**, 035432 (2003).
[20]H. Lee, Y.-W. Son, N. Park, S. Han, and J. Yu, Phys. Rev. B **72**, 174431 (2005).
[21]Y.-W. Son, M. L. Cohen, and S. G. Louie, Phys. Rev. Lett. **97**, 216803 (2006).
[22]L. Brey and H. A. Fertig, Phys. Rev. B **73**, 235411 (2006).
[23]N. M. R. Peres, A. H. Castro Neto, and F. Guinea, Phys. Rev. B **73**, 195411 (2006); **73**, 239902(E) (2006).
[24]V. Barone, O. Hod, and G. E. Scuseria, Nano Lett. **6**, 2748 (2006).
[25]D. Areshkin, D. Gunlycke, and C. T. White, Nano Lett. **7**, 204 (2007).
[26]D. Gunlycke, D. A. Areshkin, and C. T. White, Appl. Phys. Lett. **90**, 142104 (2007).
[27]F. Sols, F. Guinea, and A. H. Castro Neto, Phys. Rev. Lett. **99**, 166803 (2007).
[28]L. Pisani, J. A. Chan, B. Montanari, and N. M. Harrison, Phys. Rev. B **75**, 064418 (2007).
[29]L. Yang, C.-H. Park, Y.-W. Son, M. L. Cohen, and S. G. Louie, Phys. Rev. Lett. **99**, 186801 (2007).
[30]D. Gunlycke, J. Li, J. W. Mintmire, and C. T. White, Appl. Phys. Lett. **91**, 112108 (2007).
[31]A. Onipko, Phys. Rev. B **78**, 245412 (2008).
[32]Hengyi Xu, T. Heinzel, M. Evaldsson, and I. V. Zozoulenko, Phys. Rev. B **77**, 245401 (2008).
[33]M. Evaldsson, I. V. Zozoulenko, Hengyi Xu, and T. Heinzel, Phys. Rev. B **78**, 161407(R) (2008).
[34]A. Cresti, G. Grosso, and G. P. Parravicini, Phys. Rev. B **77**, 233402 (2008).
[35]M. Yamamoto, Y. Takane, and K. Wakabayashi, Phys. Rev. B **79**, 125421 (2009).
[36]J. Jiang, W. Lu, and J. Bernholc, Phys. Rev. Lett. **101**, 246803 (2008).
[37]S. Dutta and S. K. Pati, J. Phys. Chem. B **112**, 1333 (2008).
[38]E. R. Mucciolo, A. H. Castro Neto, and C. H. Lewenkopf, Phys. Rev. B **79**, 075407 (2009).
[39]S. Ihnatsenka, I. V. Zozoulenko, and G. Kirczenow, Phys. Rev. B **80**, 155415 (2009).
[40]S. Ihnatsenka and G. Kirczenow, Phys. Rev. B **80**, 201407(R) (2009).
[41]A. López-Bezanilla, F. Triozon, and S. Roche, Nano Lett. **9**, 2537 (2009).
[42]A. La Magna, I. Deretzis, G. Forte, and R. Pucci, Phys. Rev. B **80**, 195413 (2009).
[43]P. San-Jose, E. Prada, E. McCann, and H. Schomerus, Phys. Rev. Lett. **102**, 247204 (2009).
[44]Q. Ran, M. Gao, X. Guan, Y. Wang, and Z. Yu, Appl. Phys. Lett. **94**, 103511 (2009).
[45]H. -H. Lin, T. Hikihara, H. -T. Jeng, B. -L. Huang, Ch. -Y. Mou, and X. Hu, Phys. Rev. B **79**, 035405 (2009).
[46]S. Dutta, A. K. Manna, and S. K. Pati, Phys. Rev. Lett. **102**, 096601 (2009).
[47]J. Jung, T. Pereg-Barnea, and A. H. MacDonald, Phys. Rev. Lett. **102**, 227205 (2009).
[48]A. Ramasubramaniam, Phys. Rev. B **81**, 245413 (2010).
[49]B. Biel, F. Triozon, X. Blase, and S. Roche, Nano Lett. **9**, 2725 (2009).
[50]For a recent review see G. Kirczenow, *in*, The Oxford Handbook of Nanoscience and Technology, edited by A. V. Narlikar and Y. Y. Fu, (Oxford University Press, Oxford, 2010), vol. 1, chap. 4.
[51]V. W. Brar, Y. Zhang, Y. Yayon, T. Ohta, J. L. McChesney, A. Bostwick, E. Rotenberg, K. Horn, and M. F. Crommie, Appl. Phys. Lett. **91**, 122102 (2007).
[52]T. J. Booth, P. Blake, R. R. Nair, D. Jiang, E. W. Hill, U. Bangert, A. Bleloch, M. Gass, K. S. Novoselov, M. I. Katsnelson, and A. K. Geim, Nano Lett. **8**, 2442 (2008); A. Dato, Zonghoon Lee, Ki-Joon Jeon, R. Erni, V. Radmilovic, Th. J. Richardson, and M. Frenklach, Chem. Commun. **40**, 6095 (2009).
[53]D. Stojkovic, P. Zhang, P. E. Lammert, and V. H. Crespi, Phys. Rev. B **68**, 195406 (2003).
[54]O. Leenaerts, B. Partoens, and F. M. Peeters, Appl. Phys. Lett. **92**, 243125 (2008).
[55]O. Leenaerts, B. Partoens, and F. M. Peeters, Phys. Rev. B **80**, 245422 (2009).
[56]O. Leenaerts, B. Partoens, and F. M. Peeters, Phys. Rev. B **79**, 235440 (2009).
[57]Z. M. Ao and F. M. Peeters, J. Phys. Chem. C **114**, 14503 (2010). http://dx.doi.org/10.1021/jp103835k
[58]Z. M. Ao and F. M. Peeters, Phys. Rev. B **81**, 205406 (2010).
[59]For a recent review see A. H. Castro Neto, F. Guinea, N. M. R. Peres, K. S. Novoselov, and A. K. Geim, Rev. Mod. Phys. **81**, 109 (2009).
[60]Yu. V. Skrypnyk and V. M. Loktev, Phys. Rev. B **73**, 241402 (2006).
[61]V. M. Pereira, F. Guinea, J. M. B. Lopes dos Santos, N. M. R. Peres, and A. H. Castro Neto, Phys. Rev. Lett. **96**, 036801 (2006).
[62]T. O. Wehling, A. V. Balatsky, M. I. Katsnelson, A. I. Lichtenstein, K. Scharnberg, and R. Wiesendanger, Phys. Rev. B **75**, 125425 (2007).
[63]Yu. V. Skrypnyk and V. M. Loktev, Low Temp. Phys. **33**, 9 (2007).
[64]J. P. Robinson, H. Schomerus, L. Oroszlány, and V. I. Fal'ko, Phys. Rev. Lett. **101**, 196803 (2008).
[65]V. M. Pereira, J. M. B. Lopes dos Santos, and A. H. Castro Neto, Phys. Rev. B **77**, 115109 (2008).
[66]D. M. Basko, Phys. Rev. B **78**, 115432 (2008).
[67]T. O. Wehling, M. I. Katsnelson, and A. I. Lichtenstein, Chem. Phys. Lett. **476**, 125 (2009).
[68]T. O. Wehling, M. I. Katsnelson, and A. I. Lichtenstein, Phys. Rev. B **80**, 085428 (2009).
[69]S. S. Pershoguba, Yu. V. Skrypnyk, and V. M. Loktev, Phys. Rev. B **80**, 214201 (2009).
[70]T. O. Wehling, S. Yuan, A. I. Lichtenstein, A. K. Geim, and M. I. Katsnelson, Phys. Rev. Lett. **105**, 056802 (2010).
[71]Yu. V. Skrypnyk and V. M. Loktev, Phys. Rev. B **82**, 085436 (2010).
[72]The version of extended Hückel theory that we use here is that of J. H. Ammeter, H.-B. Bürgi, J. C. Thibeault, and R. Hoffman, J. Am. Chem. Soc. **100**, 3686 (1978) as implemented in the YAEHMOP numerical package by G. A. Landrum and W. V. Glassey (Source-Forge, Fremont, California, 2001).
[73]S. Datta, W. D. Tian, S. H. Hong, R. Reifenberger, J. I. Henderson, and C. P. Kubiak, Phys. Rev. Lett. **79**, 2530 (1997).
[74]E. G. Emberly and G. Kirczenow, Phys. Rev. Lett. **87**, 269701 (2001).
[75]E. G. Emberly and G. Kirczenow, Phys. Rev. B **64**, 235412 (2001).

[76]J. G. Kushmerick, D. B. Holt, J. C. Yang, J. Naciri, M. H. Moore, and R. Shashidhar, Phys. Rev. Lett. **89**, 086802 (2002).
[77]D. M. Cardamone and G. Kirczenow, Phys. Rev. B **77**, 165403 (2008).
[78]D. M. Cardamone and G. Kirczenow, Nano Lett. **10**, 1158 (2010).
[79]F. Demir and G. Kirczenow, J. Chem. Phys. **134**, 121103 (2011).
[80]G. Kirczenow, P. G. Piva, and R. A. Wolkow, Phys. Rev. B **72**, 245306 (2005).
[81]P. G. Piva, R. A. Wolkow, and G. Kirczenow, Phys. Rev. Lett. **101**, 106801 (2008).
[82]G. Kirczenow, P. G. Piva, and R. A. Wolkow, Phys. Rev. B **80**, 035309 (2009).
[83]J. Buker and G. Kirczenow, Phys. Rev. B **78**, 125107 (2008).
[84]J. Buker and G. Kirczenow, Phys. Rev. B **72**, 205338 (2005).
[85]M. J. Frisch, G. W. Trucks, H. B. Schlegel, G. E. Scuseria, M. A. Robb, J. R. Cheeseman, G. Scalmani, V. Barone, B. Mennucci, G. A. Petersson, H. Nakatsuji, M. Caricato, X. Li, H. P. Hratchian, A. F. Izmaylov, J. Bloino, G. Zheng, J. L. Sonnenberg, M. Hada, M. Ehara, K. Toyota, R. Fukuda, J. Hasegawa, M. Ishida, T. Nakajima, Y. Honda, O. Kitao, H. Nakai, T. Vreven, J. A. Montgomery Jr., J. E. Peralta, F. Ogliaro, M. Bearpark, J. J. Heyd, E. Brothers, K. N. Kudin, V. N. Staroverov, R. Kobayashi, J. Normand, K. Raghavachari, A. Rendell , J. C. Burant , S. S. Iyengar , J. Tomasi, M. Cossi, N. Rega, J. M. Millam, M. Klene, J. E. Knox, J. B. Cross, V. Bakken, C. Adamo, J. Jaramillo, R. Gomperts, R. E. Stratmann, O. Yazyev, A. J. Austin, R. Cammi C. Pomelli, J. W. Ochterski, R. L. Martin, K. Morokuma, V. G. Zakrzewski, G. A. Voth, P. Salvador, J. J. Dannenberg, S. Dapprich, A. D. Daniels, O. Farkas, J. B. Foresman, J. V. Ortiz, J. Cioslowski, and D. J. Fox, computer code GAUSSIAN 09, revision A.02 (Gaussian Inc., Wallingford, CT, 2009). The HSEh1PBE hybrid density functional and 6-311G(d) basis set were used in the geometry relaxations carried out in the present study.
[86]M. Igami, S. Okada, and K. Nakada, Synth. Met. **121**, 1233 (2001).
[87]P. R. Wallace, Phys. Rev. **71**, 622 (1947).
[88]S. Reich, J. Maultzsch, C. Thomsen, and P. Ordejón, Phys. Rev. B **66**, 035412 (2002).
[89]Image made with MacMolPlot program of B. M. Bode and M. S. Gordon, J. Mol. Graphics Model. **16**, 133 (1998).
[90]For a discussion of the relevant physics see E. G. Emberly and G. Kirczenow, Chem. Phys. App. A **281**, 311 (2002).
[91]E. Emberly and G. Kirczenow, Phys. Rev. Lett. **81**, 5205 (1998).
[92]E. G. Emberly and G. Kirczenow, J. Phys. Condens. Matter **11**, 6911 (1999).
[93]U. Fano, Phys. Rev. **124**, 1866 (1961).
[94]See, for example, E. N. Bulgakov and A. F. Sadreev, Phys. Rev. B **80**, 115308 (2009) and references therein.
[95]After this work was submitted for publication a similar derivation of Eq. (9) was published in Ref. 71.
[96]T. Horiguchi, J. Math. Phys. **13**, 1411 (1972).
[97]If the calculation for the model in Fig. 3 is repeated but neglecting the overlaps $\sigma_{\alpha j}$ between the EMOs and graphene $2p_z$ orbitals we find $\epsilon_{\rm DR} = -0.220t, -0.189t, -0.131t$, and $0.045t$ for F, OH, H, and O, respectively, values that differ by a few percent from those obtained in the corresponding calculations that include the overlaps $\sigma_{\alpha j}$. These differences and the corresponding differences in the strengths of the resonances are quite small because both the Dirac point resonance energies $\epsilon_{\rm DR}$ and the overlaps $\sigma_{\alpha j}$ are small and therefore the energy-dependent correction terms $-\epsilon\sigma_{\alpha j}$ to Hamiltonian matrix elements $\gamma_{\alpha j}$ that are due to the overlaps (discussed at the end of Sec. II) are small at the resonance energies.
[98]S. Y. Quek, J. B. Neaton, M. S. Hybertsen, E. Kaxiras, and S. G. Louie, Phys. Rev. Lett. **98**, 066807 (2007).
[99]The extended Hückel model as parametrized in Ref. 72 [after the application of Eq. (2)] yields the value 2.02 eV for t_{ij} for nearest-neighbor carbon atoms of undistorted pristine graphene. For consistency with the standard tight-binding model[59] of pristine graphene in which the nearest-neighbor hopping parameter $t_{ij} = t = 2.7$ eV, we therefore scale the values of t_{ij} obtained from the extended Hückel model for nearest-neighbor carbon atoms in the graphene structure that has been distorted by the presence of the adsorbate by a factor of $2.7/2.02$. No scaling is applied to the values of any other tight-binding parameters that we obtain from extended Hückel theory.
[100]R. Landauer, Philos. Mag. **21**, 863 (1970).
[101]E. N. Economou and C. M. Soukoulis, Phys. Rev. Lett. **46**, 618 (1981).
[102]D. S. Fisher and P. A. Lee, Phys. Rev. B **23**, 6851 (1981).
[103]M. Büttiker, Phys. Rev. Lett. **57**, 1761 (1986).
[104]V. M. Pereira, F. Guinea, J. M. B. Lopes dos Santos, N. M. R. Peres, and A. H. Castro Neto, Phys. Rev. Lett. **96**, 036801 (2006).
[105]The Dirac point shift has been considered previously in Ref. 60 for a simple generic model of point defects in infinite 2D graphene.
[106]V. M. Pereira, J. M. B. Lopes dos Santos, and A. H. Castro Neto, Phys. Rev. B **77**, 115109 (2008).